



Effects of Electroosmosis Flow of Bingham Plastic Fluid Induced by a Curved Microtube

Srivally Adurthy¹ · Motahar Reza¹ · Ali J. Chamkha²

Received: 3 January 2024 / Accepted: 17 April 2024
© King Fahd University of Petroleum & Minerals 2024

Abstract

This paper investigates the pressure-driven and electroosmotic flow of Bingham plastic fluid within a curved microtube in the presence of a streaming potential. Perturbation analysis is utilised to solve the governing equations and obtain approximate analytical solutions. Validation against existing literature confirms the accuracy of the approach, with highly favourable agreement observed. The electrical double-layer (EDL) distribution is analysed for various Debye lengths, perturbation parameters, curvature ratios, and zeta potentials. As curvature increases, the EDL decreases near the lower wall and increases near the upper wall. The impact of electroosmosis force, Debye lengths, perturbation parameters, curvature ratios, and ionic Peclet number on axial velocity profiles is investigated. Axial velocity increases with the electroosmotic parameter value due to a more significant axial electric force in the inner area. Additionally, velocity decreases with increasing Bingham parameter, particularly at the lower wall region, while it increases with curvature value in the upper half of the tube. Higher flow rates are observed within curved microtubes than linear ones under similar pressure gradients and cross-sectional shapes. Increasing Debye length reduces streaming potential magnitude, favouring pressure-driven flow over electroosmotic flow. Finally, the variation of electrokinetic energy conversion efficiency with curvature ratio for different Bingham parameters is analysed. Higher Bingham parameter values increase fluid viscosity, resulting in slower fluid movement, reduced streaming potential, and decreased efficiency of electrokinetic energy conversion. This study contributes to a deeper understanding of fluid dynamics within curved microtubes and offers insights into optimising energy conversion efficiency in Bingham plastic fluid systems.

Keywords Curved microtube · Bingham plastic fluid · Electroosmotic flow · EDL

List of Symbols

P	Undetermined isotropic pressure	V	Poloidal velocity
(r, θ, Φ)	Toroidal coordinates	W	Toroidal velocity
r	Radial coordinate (nm)	h	Intensity of deformation rate
θ	Poloidal angle	h_{dl}	Dimensionless deformation rate
Φ	Rotation of torus with in plane	e	Electron charge (1.6×10^{-19} Coulomb)
R	Major radius of toroidal system (μm)	n_0	Bulk electrolyte concentration (1 mol/m^{-3})
a	Radius of torus	z_+	Valence of cation
$\vec{V} = (U, V, W)$	Velocity vector	z_-	Valence of anion
U	Radial velocity	k_B	Boltzmann constant (1.38×10^{-23} J/K)
		T	Temperature (K)
		\tilde{E}_s	Streaming potential
		$\partial P / \partial \phi$	Pressure gradient
		$u = W / u_p$	Dimensionless form of W
		$u_r = u_e / u_p$	Ratio of electroosmotic velocity to pressure-driven characteristic velocity
		u_p	Pure pressure-driven nature of assumed fluid dynamic transport

✉ Motahar Reza
motaharreza90@gmail.com

¹ Department of Mathematics, GITAM Deemed to be University, Hyderabad 502329, India

² Faculty of Engineering, Kuwait College of Science and Technology, 35004 Doha, Kuwait



S	Bingham parameter (0–2)
u_0	Zeroth-order term of velocity distribution
u_1	First-order term of velocity distribution
u_r	Dimensionless-velocity scale
u_p	Normalised pressure gradient
E_s	Distribution of streaming potential
$E_{s,0}$	Streaming potential of zeroth order
$E_{s,1}$	Streaming potential of first order
I_s	Streaming current
I_c	Conduction current
M	Peclet number (0.01–10)

Greek Symbols

τ_{ij}	Stress tensor
e_{ij}	Rate of strain tensor
δ_{ij}	Yield stress tensor
ϑ	Physical constant, yield value of material
η	Variable viscosity
η_1	Reciprocal viscosity
$\delta = \frac{a}{R}$	Curvature ratio (0–2 nm)
$\tilde{\Psi}$	Overall electric potential
$\tilde{\psi}_e$	EDL potential
$\tilde{\psi}_s$	Streaming potential
$\tilde{\rho}_e$	Net charge density (1060 kg/m ³)
ε_p	Electric permittivity (5.3×10^{-19} C/Vm)
λ	Debye length
κ	Inverse of dimensionless Debye length (m ⁻¹)
$\tilde{\zeta}$	Zeta potential (0–0.5 mV)
ζ	Dimensionless zeta potential
μ	Viscosity (10 ⁻⁶ m ² /s)
λ_1, λ_2	Constants
ε	Perturbation parameter (0–1 nm)
ψ_e	Dimensionless EDL potential
ψ_0	Zeroth-order term of EDL potential
ψ_1	First-order term of EDL potential

1 Introduction

Microchannels can be divided into many types and subtypes. Different types of microchannels are compared based on their dimensions, length, channel type, material, fabrication method, fluid and fluid flow pattern, particle size, velocity, current densities, temperature, heat fluxes, flow rates, Reynolds numbers, simulation techniques, mathematical analysis, and applications. These were created by different research groups. They can be utilised to imitate

the letters of the English alphabet. Among these are the letters J, Y, T, U, and S, which have the ability to take on the appearance of any letter in the alphabet. Additional variations of microchannels that can be created encompass square, circular, triangular, double spiral, and double coil configurations. These objects also have a curved, curvilinear, and sinusoidal shape. Microchannels can be classified according to their designs and applications. Curved microchannels usually exhibit a single curvature. Researchers have utilised curved microchannels in several applications, including heat transmission, flow characteristics, mass transfer, and many more. The primary uses of straight microtubes are in protein emulsification, proton-exchange membrane fuel cells, liquid and gas transmission, haemodialysis, focussing behaviour, particle separation, and flow boiling performance.

Curved microtubes are essential in microfluidic devices because they can generate secondary flows, which improve the efficiency of mixing and separation of particles. Microtubes are commonly created utilising many microfabrication methods, including soft lithography, micro-moulding, and laser micromachining. These techniques enable the exact fabrication of complex microfluidic structures with exceptional precision and consistency. The primary constituent of the microfluidic device is the microtubes, which possess a diverse array of inlet and outlet apertures to facilitate fluid flow. These gadgets enable applications in several disciplines like as physics, and medicine. These microtubes are frequently employed in microfluidic devices and systems for a variety of applications, including lab-on-a-chip devices, biological diagnostics, chemical analysis, and microscale heat exchangers [1]. Depending on their design, curved microtubes can have a variety of curves, from slight bends to severe curves. Berger et al. [2] have investigated on flow of fluid in curved pipes. The radius of the tube and curviness of curved microtubes are important characteristics that can impact fluid flow behaviour and performance. Since the radius of the microtube is of micrometres, the flow of the fluid in these kinds of tubes is complex. As fluids flow through the curved microtube, it enhances to encourage the mixing of non-Newtonian fluids and dispersion [3]. The analytical solution for fully developed flow in a curved tube with a circular cross section under the constraint of a modest curvature ratio $\delta R = a$, where R and a are the radii of the coil and the tube, was obtained by Dean [4] and later investigated theoretically about the stability of flow of fluid between concentric under pressure [5].

Researchers have investigated the properties of fluid flow in curved microchannel by using different geometries. Mes-saris and Karaholios [6] have given an analytical solution for an unsteady fluid flow in curved pipe. Yang [7] did a experimental work based on the flow characteristics of fluid in curved microchannel with different curvature radii and

geometrical dimensions. Wang [8] has presented the analytical solution for the electroosmotic flow in the semicircular microtube and found the yield solutions by using the combination of constant zeta potential on the flat and curved wall boundaries. Ding and Jian [9] investigated the Electrokinetic flow of two layer fluids through nanochannel and later continued the investigation on energy conversion in a curved circular microtube [10]. This paper's findings show that the distribution of the electrical double-layer (EDL) potential is skewed based on the result of the microtube curvature and the EDL potential is greater on the outside than that of inside of the curve. Luo [11] investigated how the fluid is driven by the application of an external DC or AC electric field and examined the transient electroosmotic flow in a rectangular curved microtube.

The interaction of the ions in the surrounding fluid with the charged surface results in the formation of the electric double layer (EDL). The charge on the solid surface and ionic strength of the fluid and properties of fluid and solid are the terms that will affect the thickness of the EDL, and this thickness is called Debye length. The potential difference between the fluid and EDL is known as zeta potential, and it is a measure of electrostatic attraction and repulsion between the charged particles and the solid surface. Electroosmosis refers to the flow of the fluid which was induced by the externally applied electric field and EDL. Due to the applied electric field, the charged particles in the fluid move and cause the fluid to flow in opposite directions, and then, electroosmosis plays an important role to control the flow of fluid and particles. EDL plays a crucial role in both zeta potential and electroosmosis. By enhancing these effects, nowadays researchers are developing new technologies and applications for various sectors, including biotechnology, electrochemistry, and laboratory-on-chip devices.

To investigate the flow of non-Newtonian fluid in a curved micropipes is complicated due to the presence of secondary flow structures, namely Dean vortices. These structures are can vary the velocity profile and flow rate and affect the flow behaviour in the assumed microchannel. Non-Newtonian fluids exhibit various flow behaviours that differ from the straightforward linear correlation between shear stress and shear rate seen in Newtonian fluids. For instance, certain non-Newtonian fluids, like Bingham plastics, require a certain amount of pressure (referred to as yield stress) before they begin to flow. Still, other non-Newtonian fluids, such as shear-thinning fluids, demonstrate a reduction in viscosity as the shear rate rises. Norouzi and Biglari [12] have provided the analytical solution for incompressible flow of fluid using curved rectangular microchannel. Nekoubin [13] investigated the rheological behaviour of non-Newtonian fluid (power law) passing through curved rectangular microchannel by using SIMPLE finite volume method. Sun et al. [14] provided a mathematical model for the electroosmotic flow

of non-Newtonian fluid. Cheng et al. [15] have discussed about the electroviscous flow of non-Newtonian fluid and its rheology behaviour in circular microtube. Song et al. [16] have investigated on the characteristics of non-Newtonian fluid at micro-/nanoscale. Yong Guo [17] investigated the dynamic behaviour of non-Newtonian fluid when it passes through a microtube (cantilevered). Sarabandi [18] investigated about thermal analysis of power law (non-Newtonian) fluid in curved circular microchannel. Si et al. [19] studied about the flow of Oldroyd-B fluid(non-Newtonian) with electroosmotic effect in curved microchannel. Moghadam [20] investigated about the flow of electroosmosis in a circular microchannel under hydrodynamically fully developed thermal conditions. Riaz [21] elaborated the mathematical results from the exact solutions of electroosmosis through elliptical duct. Kumawat et al. [22] have investigated and analysed about the entropy generation of MHD non-Newtonian fluid flow through curved artery with heat source and chemical reaction. Sun [23] has proposed and developed the innovative cyclic and progressive electroosmosis method and verified through laboratory methods. Researchers can create innovative micro-fluidic devices and processes, which are more effective and productive by having a better understanding about the complex interaction between the fluid's non-Newtonian characteristics and the geometry of the channel.

The study of non-Newtonian fluids has become more important due to its wide range of industrial and technological applications. Viscoplastic fluids, a type of non-Newtonian fluids, have a yield stress and so demonstrate characteristics of both solids and liquids in various flow conditions. The constitutive equations of Bingham plastic fluid were discovered in the history of rheology. However, the specific features of the flow field of Bingham plastic fluid remain mostly unknown in present times. The experimental study conducted previously provided an accurate answer for the stable laminar flow of Bingham plastic fluid in a straight pipe. Only a limited number of academics have endeavoured to formulate the analytical representation of the turbulent movement of Bingham plastic fluid. The primary goal is to propose a methodology for predicting the behaviour of non-Newtonian fluids (specifically Bingham fluids) flowing through curved microtubes. These fluids have various applications in the chemical industry. The aim is to avoid the costly experimentation of these systems by using predictive models. Analytical studies were conducted on the flow of Bingham plastic fluids through coiled pipes with circular cross sections. A non-Newtonian fluid with a yield stress—the lowest stress that must be applied to a fluid before it starts to flow, is called a Bingham plastic fluid. The idea of yield stress was first given by Shwedov [24]. Subsequently, Bingham [25] introduced the flow shear diagram, which illustrates a direct correlation

between stress and strain, in order to elucidate the characteristics of plastic. Barnes [26] carried out a comprehensive analysis of the viscoplastic properties of materials. Paste, paint, slurries and food substances like margarine, mayonnaise come under the examples of Bingham plastic fluids. Once the yield stress is exceeded, the fluid flows like a Newtonian fluid with a constant viscosity. Clegg and Power [27] developed a successive approximations for the flow of Bingham plastic fluid in a slightly curved pipe using perturbation analysis and investigated the thickness of plug flow in the centre of the pipe. Velocity profile for the pressure-driven Bingham plastic fluid around two-dimensional concentric annulus was investigated by Roberts and Cox [28] and provided the validated result that how channel curvature would affect the pressure gradient needed to start a flow at a particular yield stress as well as the breadth of the plug region and the flux through the channel at various angles of curvature. Shojaeian et al. [29] had an experimental investigation based on the flow of non-Newtonian fluid and convective heat transfer in microtubes. Karabi and Moghadam [30] have investigated about the flow of non-Newtonian fluid in semi-circular microtubes and concluded that the active flow within the electric double layer (EDL) drags the rest of the liquid due to frictional forces arising from the fluid viscosity, and consequently a plug-like velocity profile is attained. Tada [31] studied experimentally about the flow of kaolin clay slurries (Bingham plastic fluid) in coiled pipes with circular cross section and made it clear that the curvature of the pipe will be greater when the concentration of slurry is higher. Ali Jabari and Pooria [32] have investigated the flow Carreau–Yasuda model (non-Newtonian fluid) in curved microtube with electroosmosis as an external force. Recently, Philippe Beltrame [33] studied about the axisymmetric flow of fluid in a microtube driven by a force in the axis of tube. Kumar et al. [34] had a numerical investigation of non-Newtonian fluid through curved melting sheet with buoyancy forces.

Researchers in the microfluidics and biological fields have been very interested in microtubes made from microelectromechanical systems (MEMS) for the past forty years. Understanding the behaviour of Bingham plastic fluids in microfluidic systems is crucial for industries dealing with complex fluids, such as food processing, cosmetics, and pharmaceuticals. The study provides insights into how these fluids behave under the influence of electroosmosis in confined geometries, which can help optimise processes and product formulations. By investigating the behaviour of these complex fluids under the influence of electroosmosis, the research provides insights into controlling flow in microfluidic devices, which is crucial for applications in lab-on-a-chip devices, drug delivery systems, and microscale chemical reactors. Understanding how electroosmosis affects the flow of Bingham plastic fluids in curved geometries is essential for optimising these devices performance and

designing more efficient microfluidic systems. The findings could lead to advancements in microfluidic technologies and have significant implications for various industries, including biotechnology, medicine, and chemical engineering. Research findings indicate that blood can be classified as a Casson fluid or a Bingham plastic fluid with a finite yielding stress from a rheological perspective. The specific limitations of these classifications enable accurate modelling of fluid behaviour, particularly in the case of Bingham fluids. This has significant applications in various industrial processes, such as fluid displacement, leading to cost and time savings. To further validate the effectiveness of this method with complex fluids like turbulent flows, it would be beneficial to conduct simulations.

Ng and Ni [35] investigated the relation between rheological parameters of the material and the zeta potential which affected the reduction of Electroosmotic velocity caused by yield stress. Bhandari et al. [36] have considered the linear viscoplastic fluid model to analyse the effects of viscoplastic in the membrane-based pumping flow through the microchannel and also found rheological effects of fluid flow and pumping characteristics. Zhang et al. [37] clarified the mechanisms of Bingham plastic fluid with electroviscous effects in a micro-sized circular tube and found that the Bingham behaviour reduces the strength of electroviscous and electroviscous effect increases the width of the flow core. Shahsavari and Mckinley [38] presented the theoretical and numerical solution about the steady flow of viscoplastic fluids passing through fibrous media. Recently, Panwar [39] investigated numerically about the flow of Bingham plastic fluid in serpentine tube with a circular cross section in order to gain a greater understanding of the flow behaviour, slip and no-slip conditions by using set of parameters. Al-Mdallal et al. [40] have recently worked on pseudoplastic fluid through a circular cylinder by using Keller box calculation (implicit finite differences). Yang et al. [41] have discussed about the effects of the relative roughness, the fractal dimension, and the fractional derivative order on frictional resistance of non-Newtonian fluid in microtubes and later continued investigation on the characteristics of flow of Maxwell fluid with the effect of electroosmosis in microtube [42]. Kontaxi et al. [43] have studied the properties and development of air bubbles in microtubes subjected to the passage of non-Newtonian fluids. Reza et al. [44] have investigated numerically about the anisotropic property of turbulent flow of blood through multiple stenosed microtube.

Bingham fluid behaves elastically under lower stresses and maintains its shape, but under higher stresses, it transitions to a plastic flow state where it can deform and flow while maintaining a constant viscosity. The yield point is the critical stress at which a material changes from an elastic to a plastic state. The main focus of this paper is on areas characterised by plastic flow rather than those exhibiting

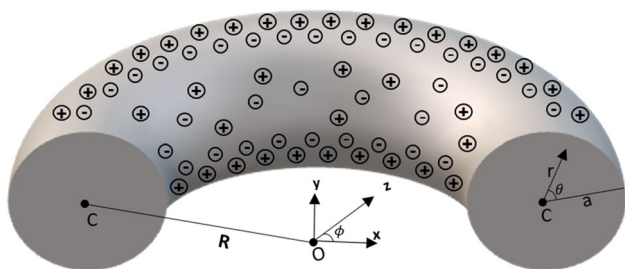


Fig. 1 Sketch of the physical problem and related coordinate systems

elastic-solid behaviour. Oldroyd [45] formulated the equation of state for such material, and it is given by usual summation convention as

$$\tau_{ij} = -P\delta_{ij} + 2\eta e_{ij}. \tag{1}$$

The variable viscosity involves two constants, i.e. reciprocal mobility η_1 and yield stress tensor $\vartheta_{ij} = \vartheta e_{ij}$. Stress tensors and rate of strain tensor are denoted by τ_{ij} , e_{ij} and P is the undetermined isotropic pressure that applies on fluid element, where

$$\eta = \eta_1 + \vartheta (2e_{ij}e_{ij})^{-\frac{1}{2}}. \tag{2}$$

Substituting Eq. (2) in Eq. (1), then

$$\tau_{ij} = -P\delta_{ij} + 2\eta_1 e_{ij} + \frac{2\vartheta e_{ij}}{(2e_{ij}e_{ij})^{\frac{1}{2}}}. \tag{3}$$

The index $-\frac{1}{2}$ indicates the positive reciprocal square root. Hence, when a Bingham solid is in a flowing state, it can be considered as a fluid characterised by a variable viscosity η . This viscosity is a scalar function of the stress tensor (or rate of strain tensor), which includes two physical constants η_1 and ϑ .

An analytical solution for the fully developed electroosmotic flow of Bingham plastic fluid passing through curved microtube is given. The walls of the microtube carry zeta potential. By using the perturbation analysis, we found the effects of EDL potential, axial velocity, flow rate, streaming potential, and electrokinetic energy conversion. The effects of governing parameters such as curvature ratio, Bingham parameter, and inverse EDL thickness are studied in detail.

2 Mathematical Model

Figure 1 illustrates the visual representation of the toroidal coordinate system, described using the coordinates (r, θ, ϕ) . 'r' represents the radial coordinate, which signifies the distance from the centre of the torus to any point on the cross

section of the torus. 'θ' represents the poloidal angle, determining the rotation or position of any point within the circular cross section of the torus. 'φ' represents the rotation of the torus within the plane. 'C' and 'a' denote the centre and radius of the torus, respectively. Here, 'R' indicates the major radius of the toroidal system, representing the distance from the centre of the torus to the centreline of the torus. The curvature ratio is denoted by $\delta = a/R$.

By considering the given geometry, line element is given by [27]:

$$ds^2 = dr^2 + r^2 d\theta^2 + (R + r \sin \theta)d\phi^2. \tag{4}$$

The toroidal coordinate system can also be conceptualised as a curvilinear coordinate system with a circular cross section. The diameter of the analysed microtube is measured in micrometres, while its length is approximately within the range of 10 μm.

The flow is assumed to be unidirectional, steady-state, and fully developed. This study focuses on plastic viscosity rather than elastic viscosity. The motion of a viscous incompressible Bingham plastic fluid is assumed within the microtube. It is assumed that the velocity components are $\tilde{V} = (U, V, W)$, where (U, V, W) represents the radial velocity, the poloidal velocity, and the toroidal velocity and all dependent on (r, θ) and independent on ϕ . The stress tensors and the rate of strain tensors have been mentioned. The thickness of the electric double layer (EDL) is expressed in nanometres. Even a thin EDL affects the flow, and the distribution of electric potential is influenced by various parameters, including factors such as surface charge density, ionic strength, and the curvature of the tube. For Bingham plastic fluids, the term "movable fluid radius" denotes the distance from the centreline of flow to the point where the fluid starts movement or deformation in response to applied stress. Understanding the flow behaviour of Bingham plastic fluids in different geometries, such as curved microtubes or channels, is essential. When Bingham plastic fluids pass through a restricted area like a microtube, the fluid close to the centreline can travel without obstruction, but the fluid near the walls holds still until a specific level of stress is exerted. The moveable fluid radius delineates the boundary between the area of the fluid that are in motion and stationary region of the fluid. Understanding the movable fluid radius is crucial for forecasting significant flow properties, such as pressure reduction and velocity distribution. It aids engineers and researchers in maximising the efficiency of systems that include Bingham plastic fluids.

2.1 Electric Potential Distribution

When a fluid containing ions is compelled to flow through a curved microtube, the tube's curvature can lead to an accumulation of ions on the inner wall. This accumulation gives

rise to the formation of an electric double layer (EDL). The EDL comprises two distinct layers: the Stern layer, consisting of ions tightly bound to the surface, and the diffuse layer, composed of ions loosely connected and extending into the fluid's bulk. These two layers collectively constitute the electric double layer. The presence of the EDL can significantly influence both the fluid's flow characteristics and the distribution of electrostatic potential within the tube.

$$\nabla^2 \tilde{\Psi} = -\frac{\tilde{\rho}_e}{\varepsilon_p} \tag{5}$$

The above equation is also called Poisson equation. When an electrolyte solution moves through a microchannel due to an applied pressure difference, net charges in the EDL move, which creates an electric current. This current is called the streaming current. Also, as charges build up at the channel downstream and a forced electrical potential difference, known as the streaming potential. It is created between the ends of the microchannel. In microchannels, setting up the streaming current and streaming potential is a way of transforming hydraulic energy into electrical power. Since the flow is driven by pressure gradient, the net charges in the fluid flow in the curved microtube lead to streaming potential. By electrostatic theory, the electric potential $\tilde{\Psi}$ refers the overall density, i.e. combination of both electric potential field $\tilde{\psi}_e$ (EDL potential) and streaming potential $\tilde{\psi}_s$.

$$\tilde{\Psi} = \tilde{\psi}_e + \tilde{\psi}_s, \tag{6}$$

where $\tilde{\rho}_e$ is the net charge density, ε is electric permittivity, and ∇^2 is a Laplacian operator, i.e. $\nabla^2 = \hat{e}_r \frac{\partial}{\partial r} + \hat{e}_\theta \left(\frac{1}{r} \frac{\partial}{\partial \theta} \right) + \hat{e}_\phi \left(\frac{1}{(R+r \sin \theta)} \frac{\partial}{\partial \psi} \right)$.

Therefore, Eq. (5) can be written as:

$$\nabla^2 (\tilde{\psi}_e + \tilde{\psi}_s) = -\frac{\tilde{\rho}_e}{\varepsilon_p} \tag{7}$$

Since the flow is around z -axis, EDL potential is independent of toroidal angle- ϕ , i.e. $\tilde{\psi}_e(r, \theta)$, and streaming potential is dependent on toroidal angle- ϕ , i.e. $\tilde{\psi}_s(\phi)$ [10].

$$\nabla^2 (\tilde{\psi}_e(r, \theta) + \tilde{\psi}_s(\phi)) = -\frac{\tilde{\rho}_e}{\varepsilon_p}, \tag{8}$$

$$\nabla^2 \tilde{\psi}_e(r, \theta) + \nabla^2 \tilde{\psi}_s(\phi) = -\frac{\tilde{\rho}_e}{\varepsilon_p} \tag{9}$$

The streaming potential in the above equation is considered as:

$$\tilde{\psi}_s(\phi) = \psi_0 - zE_0(t) \tag{10}$$

where ψ_0 is the reference potential at the inlet of the tube at $z = 0$ and $\psi_0 - zE_0(t)$ is the streaming potential at a given axial position in the microtube obtained due to strength of electric field E_0 in the absence of EDL, and according to assumption of the problem, E_0 is independent of position and time [10]. Therefore,

$$\nabla^2 \tilde{\psi}_s(\phi) = 0. \tag{11}$$

By substituting Eq. (11) in Eq. (9), we obtain

$$\nabla^2 \tilde{\psi}_e(r, \theta) = -\frac{\tilde{\rho}_e}{\varepsilon_p}, \tag{12}$$

$$\tilde{\rho}_e = e(z_+n_+ + z_-n_-) = ez_v(n_+ - n_-), \tag{13}$$

$$\text{where } n_{\pm} = n_0 \exp\left(\mp \frac{z_v e \tilde{\psi}_e}{k_B T}\right). \tag{14}$$

Here e is the electron charge, n_0 is the bulk electrolyte concentration, z_+ is the valence of cation and z_- is the valence of anion, k_B is the Boltzmann constant, and T is the temperature.

By substituting Eq. (14) in (13), the obtained result should substitute in (9), which leads to the Poisson–Boltzmann equation

$$\nabla^2 \tilde{\psi}_e = \frac{2n_0 z_v e}{f_p} \left(\sinh\left(\frac{z_v e \tilde{\psi}_e}{k_B T}\right) \right). \tag{15}$$

In toroidal coordinate system, Eq. (15) can be expressed as:

$$\frac{\partial^2 \tilde{\psi}_e}{\partial r^2} + \frac{1}{r} \frac{\partial \tilde{\psi}_e}{\partial r} + \frac{\sin \theta}{(R+r \sin \theta)} \frac{\partial \tilde{\psi}_e}{\partial \theta} + \frac{1}{r^2} \frac{\partial^2 \tilde{\psi}_e}{\partial \theta^2} + \frac{\cos \theta}{r(R+r \sin \theta)} \frac{\partial \tilde{\psi}_e}{\partial \theta} = \frac{2n_0 z_v e}{\varepsilon_p} \left(\sinh\left(\frac{z_v e \tilde{\psi}_e}{k_B T}\right) \right). \tag{16}$$

The above equation subjects to the boundary condition

$$\tilde{\psi}_e(r, \theta) = \tilde{\zeta} \text{ at } r = a, \tag{17}$$

here represents the zeta potential. Now, Eq. (11) can be expressed in coordinate system as

$$\frac{d^2(\tilde{\psi}_s)}{d\phi^2} = 0. \tag{18}$$

Equation (18) implies that $\frac{d(\tilde{\psi}_s)}{d\phi}$ is constant. Along the centreline of the torus, radius is equal to 0 and let us assume

the magnitude of electric field strength, which is related to streaming potential as

$$\tilde{E}_s = -\frac{1}{R} \left(\frac{d\tilde{\psi}_s}{d\phi} \right). \tag{19}$$

3 Mathematical Formulation of Physical Model

3.1 Governing Equations of Fluid Motion

The fluid movement is viewed as steady and occurring in a unidirectional within a curved microtube. This microchannel is defined by a uniform curvature. The flow is influenced by combination of pressure gradient and electroosmosis. The pressure-driven and electroosmotic flows can be made to regulate each other. The fluid motion is driven by a constant pressure gradient along the ϕ direction. When fluid moves in a curved microtube along a stream line, it moves along the line of the microtube and also moves in the plane of the cross section. The secondary motion slows down the flow rate caused by a given pressure gradient and moves the location where the primary motion is greatest. It is clear that the pressure in the middle of the microtube has greater influence on the deflection. We have considered the flow Bingham plastic fluid through a circular microtube, the diameter of the analysed microtube is measured in micrometres, while its length is approximately within the range of 10 μm and the thickness of EDL is considered to be in nanometres. Since the radius of the microtube is in terms of micrometres and also comparing the order of magnitude of stream-wise velocity, we neglect the flow through U, V direction and considering the assuming the axial direction to flow the fluid in the W -direction. Therefore, the axial velocity component W is dependent on (r, θ) and independent of ϕ . Also, with the assumption of low Reynolds number, the viscous forces will be dominant compared to inertial forces. This makes the flow to be laminar throughout the channel.

Both the continuity equation and the momentum equation serve to depict the behaviour of fluids, whether they are Newtonian or non-Newtonian. The flow can be described using the Navier–Stokes equation, which is augmented with an additional electric body force, alongside the continuity equation, applicable to an incompressible fluid. Given our consideration of the Bingham plastic fluid (a non-Newtonian fluid), a nonlinear relationship between shear stress and strain rate [46] exists.

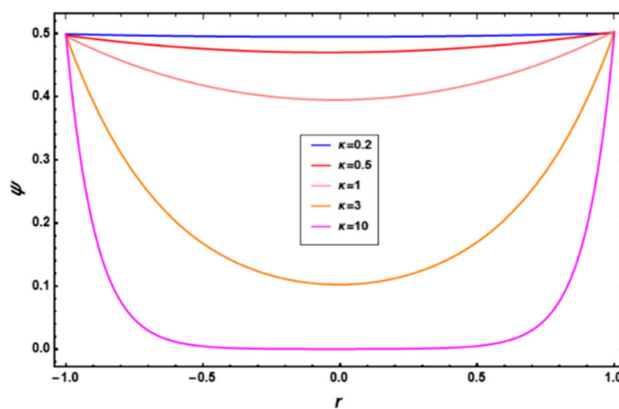


Fig. 2 Variations of EDL distribution for different values of Debye lengths

The following equations represent the continuity and momentum equations:

$$\rho \frac{\partial(u_i)}{\partial x_i} = 0, \tag{20}$$

$$\rho \frac{\partial(u_i u_j)}{\partial x_j} = \frac{\partial \tau_{ij}}{\partial x_j} + f_i. \tag{21}$$

Here \tilde{V} is the fluid velocity vector, and it is represented as $\tilde{V} = (U, V, W)$. ρ is the fluid density, p is the pressure, f_i is the electric body force and τ_{ij} represent the stress tensor, derived in Sect. 1

By considering toroidal coordinate system presented in Fig. 2, the flow velocity vector is dependent on (r, θ) and independent of toroidal angle (ϕ); the continuity equation and momentum equation reduce to the following form of equation [27, 47].

$$\frac{\partial U}{\partial r} + \frac{U}{r} + \frac{U \sin \theta}{R + r \sin \theta} + \frac{1}{r} \frac{\partial V}{\partial \theta} + \frac{V \cos \theta}{R + r \sin \theta} = 0, \tag{22}$$

$$\begin{aligned} U : \rho & \left(U \frac{dU}{dr} + \frac{V}{r} \frac{dU}{d\theta} - \frac{V^2}{r} - \frac{W^2 \sin \theta}{R + r \sin \theta} \right) \\ & = \frac{\partial}{\partial r} (\tau_{rr}) + \left(\frac{\tau_{rr} - \tau_{\theta\theta}}{r} \right) + \left(\frac{\tau_{r\theta} \cos \theta}{R + r \sin \theta} \right) + \frac{1}{r} \frac{\partial}{\partial \theta} (\tau_{r\theta}) \\ & + \left(\frac{\tau_{rr} - \tau_{\theta\theta}}{R + r \sin \theta} \right) + \frac{1}{R + r \sin \theta} \frac{\partial}{\partial \phi} (\tau_{r\phi}) + F_U, \end{aligned} \tag{23}$$

$$\begin{aligned} V : \rho & \left(U \frac{dV}{dr} + \frac{V}{r} \frac{dV}{d\theta} + \frac{UV}{r} - \frac{W^2 \cos \theta}{R + r \sin \theta} \right) \\ & = \frac{\partial}{\partial r} (\tau_{r\theta}) + \left(\frac{2}{r} + \frac{\sin \theta}{R + r \sin \theta} \right) (\tau_{r\theta}) + \frac{1}{r} \frac{\partial}{\partial \theta} (\tau_{r\theta}) \\ & + \left(\frac{\tau_{\theta\theta} - \tau_{\phi\phi}}{R + r \sin \theta} \right) + \frac{1}{R + r \sin \theta} \frac{\partial}{\partial \phi} (\tau_{\phi\theta}) + F_V, \end{aligned} \tag{24}$$

$$\begin{aligned}
 W : \rho & \left(U \frac{dW}{dr} + \frac{V}{r} \frac{dW}{d\theta} + \frac{UV \sin\theta}{R+r\sin\theta} + \frac{VW \cos\theta}{R+r\sin\theta} \right) \\
 & = \frac{\partial}{\partial r} (\tau_{r\phi}) + \left(\frac{1}{r} + \frac{2\sin\theta}{R+r\sin\theta} \right) (\tau_{r\phi}) + \frac{1}{r} \frac{\partial}{\partial \theta} (\tau_{\phi\theta}) \\
 & \quad + \frac{2\tau_{\phi\theta} \cos\theta}{R+r\sin\theta} + \frac{1}{R+r\sin\theta} \frac{\partial}{\partial \phi} (\tau_{\phi\phi}) + F_W
 \end{aligned} \tag{25}$$

Here the rate of strain tensors is denoted by e_{ij} and stress tensors are denoted by τ_{ij} . The force, denoted by $F = (F_U, F_V, F_W)$, represents the impact exerted on the body by the electric field acting upon the free ions within the electrodynamic droplet (EDL). Here $F = \tilde{\rho}_e \tilde{E}$. They are represented by the following form [27].

$$\begin{aligned}
 e_{rr} & = \frac{\partial U}{\partial r}; e_{\phi\phi} = \frac{U \sin\theta + V \cos\theta}{R+r \cos\theta}; \\
 e_{\theta\theta} & = \frac{1}{r} \frac{\partial V}{\partial \theta} + \frac{U}{r}; e_{r\theta} = \frac{1}{2} \left(\frac{1}{r} \frac{\partial V}{\partial r} + \frac{1}{r} \frac{\partial U}{\partial \theta} \right); \\
 e_{r\phi} & = \frac{1}{2} \left(\frac{\partial W}{\partial r} - \frac{W \sin\theta}{R+r \sin\theta} \right); \\
 e_{\theta\phi} & = \frac{1}{2} \left(\frac{1}{r} \frac{\partial W}{\partial \theta} - \frac{W \cos\theta}{R+r \sin\theta} \right) \\
 \tau_{rr} & = -P; \tau_{\theta\theta} = -P; \tau_{\phi\phi} = -P; \tau_{r\theta} = -P; \\
 \tau_{r\phi} & = \left(\eta_1 + \frac{\vartheta}{h} \right) \left(\frac{\partial W}{\partial r} - \frac{W \sin\theta}{R+r \sin\theta} \right) \\
 \tau_{\theta\phi} & = \left(\eta_1 + \frac{\vartheta}{h} \right) \left(\frac{1}{r} \frac{\partial W}{\partial \theta} - \frac{W \cos\theta}{R+r \sin\theta} \right),
 \end{aligned} \tag{26}$$

where η_1 represents constant reciprocal mobility and h represents the intensity of deformation rate [46]. The derivations of η_1 and h are given in ‘‘Appendix A’’.

We assume Eq. (25) for the further calculation. The terms related to toroidal angle in stress tensors and terms U, V (since $U = 0, V = 0$) will be neglected. By substituting the relevant stress tensors [27], Eq. (25) can be reduced to

$$\begin{aligned}
 & \left(\eta_1 + \frac{\vartheta}{h} \right) \left[\left\{ \left(\frac{\partial}{\partial r} + \frac{1}{r} + \frac{2\sin\theta}{R+r\sin\theta} \right) \left(\frac{\partial W}{\partial r} - \frac{W \sin\theta}{R+r\sin\theta} \right) \right\} \right. \\
 & \quad \left. + \left\{ \left(\frac{1}{r} \frac{\partial}{\partial \theta} + \frac{2\cos\theta}{R+r\sin\theta} \right) \left(\frac{1}{r} \frac{\partial W}{\partial \theta} - \frac{W \cos\theta}{R+r\sin\theta} \right) \right\} \right] \\
 & - \frac{1}{R+r\sin\theta} \frac{\partial P}{\partial \phi} - \frac{\tilde{\rho}_e}{R+r\sin\theta} \frac{\partial \tilde{\psi}_s}{\partial \phi} = 0.
 \end{aligned} \tag{27}$$

Here the curved microtube is smooth and there is no-slip condition. The boundary condition for the above equation is:

$$W = 0 \text{ at } r = a. \tag{28}$$

Therefore, Eqs. (16) and (27) illustrate the dimensionlised EDL distribution potential and the axial velocity distribution

with the respective boundary conditions (17) and (28). Now, we introduce the dimensionless terms to make those equations into non-dimensional distributions.

$$\begin{aligned}
 \zeta & = \frac{z_v e \tilde{\zeta}}{k_B T}, \quad \psi_e = \frac{z_v e \tilde{\psi}_e}{k_B T}, \quad \rho_e = \frac{z_v e a^2 \tilde{\rho}_e}{\epsilon k_B T}, \quad r' = \frac{r}{a}, \quad \kappa = \frac{a}{\lambda}, \\
 u & = \frac{w}{u_p}, \quad u_r = \frac{u_e}{u_p}, \quad E_s = \frac{\tilde{E}_s}{E_0}, \quad u_p = - \left(\frac{a^2}{\mu R} \right) \left(\frac{\partial P}{\partial \phi} \right), \\
 u_e & = - \left(\frac{\epsilon k_B T}{z_v e} \right) \left(\frac{E_0}{\mu} \right),
 \end{aligned} \tag{29}$$

where $\lambda = \left(\frac{\epsilon k_B T}{2n_0 z_v^2 e^2} \right)^{\frac{1}{2}}$ represent Debye length and κ is the inverse of the dimensionless Debye length, ζ represents the normalised zeta potential, ψ_e denotes the normalised EDL potential, ρ_e represents normalised net charge density, E_0 is the strength of characteristic electric field, u_e denotes the electroosmotic velocity. The subscript ‘ p ’ in u_p represents pure pressure-driven nature of the assumed fluid dynamic transport and u_p emphasises a normalised pressure gradient. Since the Reynolds number is less, i.e. $O(\text{Re}) \approx 1$, inertial forces will be less compared to viscous forces. Therefore, pressure gradient will be constant along the flow direction. From non-dimensional terms, it is clear that the u is a non-dimensional ($u = \frac{w}{u_p}$), where u_p is included, u_p indicates the non-dimensional pressure gradient term. This indicates that in main velocity equation, the pressure gradient term is also included, where pressure gradient is constant.

$$h_{dl} = \frac{u_p}{a} \left(\frac{du}{dr} - u \delta \sin\theta (1 - \delta r \sin\theta) \right) \approx \frac{u_p}{a} \left(\frac{du}{dr} - u \delta \sin\theta \right), \tag{30}$$

where h_{dl} represent the dimensionless of h and here we neglect higher-order terms of δ i.e., $(1 + \delta r \sin\theta)^{-1} \approx (1 - \delta r \sin\theta)$

The dimensionless form of EDL potential distribution and its boundary condition is represented as follows:

$$\frac{\partial^2 \psi_e}{\partial r^2} + \frac{1}{r} \frac{\partial \psi_e}{\partial r} + \delta \sin\theta \frac{\partial \psi_e}{\partial r} + \frac{1}{r^2} \frac{\partial^2 \psi_e}{\partial \theta^2} + \frac{\delta \cos\theta}{r} \frac{\partial \psi_e}{\partial \theta} = \kappa^2 \psi_e. \tag{31}$$

The boundary condition is reduced to

$$\psi_e(r, \theta) = \zeta a r = 1 \tag{32}$$

The dimensionless form of axial velocity distribution and its boundary condition is represented as follows:

$$\left(1 + S \left(\frac{\partial u}{\partial r} + u \delta \sin\theta \right) \right) \left(\frac{\partial^2 u}{\partial r^2} + \frac{1}{r^2} \frac{\partial^2 u}{\partial \theta^2} + \frac{1}{r} \frac{\partial u}{\partial r} \right)$$

$$\begin{aligned}
 &+ \delta \left(1 + S \frac{\partial u}{\partial r} \right) \left(\left(\frac{\partial u}{\partial r} \right) \sin \theta + \left(\frac{1}{r} \frac{\partial u}{\partial \theta} \right) \cos \theta \right) \\
 &+ (1 - \delta r \sin \theta) \left(1 + u_r E_s k^2 \psi_e \right) = 0, \tag{33}
 \end{aligned}$$

where S is a Bingham parameter. The boundary condition is written as:

$$u(r, \theta) = 0 \text{ at } r = 1. \tag{34}$$

The detailed derivation of converting dimension EDL potential distribution and axial velocity distribution to dimensionless are given in “Appendix B”.

3.2 Perturbation Method

In Eqs. (31) and (33), the two main parameters are δ and S , which represents the Bingham parameter and curvature ratio. These equations will simplify into the classical equations describing electrokinetic flux in a straight pipe when S, δ are negligible. The parameters S, δ are crucial in curved tube flow and serve as a measure of the influence of geometry. Since both the equations contain second-order partial derivatives, it is highly complicated to solve analytically. So, to solve these equations we use perturbation method and the parameters are considered to be smaller as $S = \epsilon \lambda_1, \delta = \epsilon \lambda_2$ to make the calculations simple and easy. Now, ϵ serves as perturbation parameter for the further process. A regular perturbation expansion for relevant variables can be used to define the solution for small values, as shown below.

$$\psi_e = \psi_0(r) + \epsilon \psi_1(r, \theta) + O(\epsilon^2), \tag{35}$$

$$u = u_0(r) + \epsilon u_1(r, \theta) + O(\epsilon^2), \tag{36}$$

$$E_s = E_{s,0} + \epsilon E_{s,1} + O(\epsilon^2). \tag{37}$$

These extensions estimate how the curvature ratio affects velocity field, flowrate, streaming potential. According to Eq. (35) and Eq. (36), the zero-order term describes the state in which the curve has no effect on the flow field (i.e. straight tube), while the first-order term in the series expansion describes about the flow of fluid in a slight curve microtube. Due to the application of external pressure-driven transport, Eq. (37) denotes the distribution of streaming potential. The additional higher-order components in this series describe how the perturbation solution deviates from the direction of straight duct flow.

3.2.1 Solution of Order ϵ^0

In order to obtain the zeroth-order term for the EDL potential, substitute Eq. (35) in Eq. (31), and to obtain velocity

distribution, substitute Eqs. (35), (36) in Eq. (33). The resultant equations can be obtained as follows. Now, the partial differential equations yield to differential equations of ϵ^0 .

$$\text{Order of } \epsilon^0 : \frac{d^2 \psi_0}{dr^2} + \frac{1}{r} \frac{d\psi_0}{dr} = \kappa^2 \psi_0, \tag{38}$$

$$\text{Order of } \epsilon^0 : \left(\frac{d}{dr} + \frac{1}{r} \right) \frac{du_0}{dr} + \left(1 - u_r E_{s,0} \kappa^2 \psi_0 \right) = 0. \tag{39}$$

Due to its axi-symmetry of EDL potential and velocity distribution in zeroth order, ψ_0 and u_0 are independent of θ . As a result, we only consider ψ_0 and u_0 to be a function of r . As a consequence, we can focus solely on considering ψ_0 and u_0 as functions of the radial coordinate r . With these conditions in mind, we can establish the appropriate boundary conditions as follows:

$$\begin{aligned}
 \psi_0 &= \zeta \text{ at } r = 1, \\
 u_0 &= 0 \text{ at } r = 1.
 \end{aligned} \tag{40}$$

Considering the above boundary conditions (40), we can solve Eqs. (38) and (39) easily by using Mathematica. The solution of zeroth-order term of both EDL distribution and velocity distribution is obtained as:

$$\psi_0 = \varphi \frac{I_0(kr)}{I_0(k)}, \tag{41}$$

$$u_0 = \frac{1 - r^2}{4} + \varphi u_r E_{s,0} \left(\frac{I_0(kr)}{I_0(k)} - 1 \right) \tag{42}$$

These solutions are obtained by using Bessel’s function concept. Here I_0 refers to the modified Bessel function of the first kind with a zeroth-order input.

3.2.2 Solution of Order ϵ^1

Following the same process, we need to obtain the first-order terms of ϵ .

$$\text{Order of } \epsilon^1 : \frac{\partial^2 \psi_1}{\partial r^2} + \frac{1}{r} \frac{\partial \psi_1}{\partial r} + \sin \theta \frac{d\psi_0}{dr} + \frac{1}{r^2} \frac{\partial^2 \psi_1}{\partial \theta^2} = \kappa^2 \psi_1, \tag{43}$$

$$\begin{aligned}
 \text{Order of } \epsilon^1 : & \left(\left(\lambda_1 \frac{du_0}{dr} \right) \left(\frac{d^2 u_0}{dr^2} + \frac{1}{r} \frac{du_0}{dr} \right) \right) \\
 & + \left(\frac{\partial^2 u_1}{\partial r^2} + \frac{1}{r^2} \frac{\partial^2 u_1}{\partial \theta^2} + \frac{1}{r} \frac{\partial u_1}{\partial r} \right) \\
 & + (\lambda_2 \sin \theta) \left(\frac{du_0}{dr} + r \left(-1 + u_r E_{s,0} k^2 \psi_0 \right) \right) \\
 & - u_r E_{s,0} k^2 \psi_1 = 0.
 \end{aligned} \tag{44}$$

Both ψ_1 and u_1 are dependent on r and θ . So, the derivatives of ψ_1 and u_1 are partial derivatives and ψ_0 and u_0 are only dependent on r , they are represented with normal derivatives. The boundary conditions related to Eqs. (43) and (44) are:

$$\begin{aligned} \psi_1(r, \theta) &= 0 \text{ at } r = 1, \\ u_1(r, \theta) &= 0 \text{ at } r = 1. \end{aligned} \tag{45}$$

Considering the above boundary conditions (45) and zeroth-order solutions, we have to solve Eqs. (43) and (44). Since Eq. (43) is having second-order partial derivative and Eq. (39) is a combination of both second-order partial derivative and normal derivative, it is not easy to solve. So, initially we assume a relevant solution of ψ_1 and u_1 . We substitute them in Eqs. (43) and (44), which satisfies the solution. The assumed solution of first-order term of both EDL distribution and velocity distribution is given as:

$$\psi_1(r, \theta) = f_1(r)\sin\theta, \tag{46}$$

$$u_1(r, \theta) = U_1(r)\sin\theta + U_2(r). \tag{47}$$

By substituting the $\psi_1(r, \theta)$ in Eq. (43), it changes from partial differential to normal differential equations as

$$r^2 \frac{d^2 f_1}{dr^2} + r \frac{df_1}{dr} - (1 + \kappa^2 r^2) f_1 = -\kappa r^2 \zeta \left(\frac{I_1(\kappa r)}{I_0(k)} \right), \tag{48}$$

$$\text{where } f_1(r) = \sum_{n=1}^{\infty} \left(\frac{2\zeta \left(\frac{k}{I_0(k)} \int_0^1 r I_1(kr) J_1(\mu_n, 1r) \right)}{(\mu_{n,1}^2 + \kappa^2) J_0(\mu_n, 1)} \right) J_1(\mu_n, 1r).$$

Here, J_1 denotes the first kind of ν th-order Bessel function, and $\mu_{n,1}$ is the first positive root of $J_1(r)$. We have limited to two summations for further execution of problem.

In a similar manner, substitute Eq. (46) in Eq. (44). After substitution and solving, separate the coefficient of $\sin\theta$ and constant. The coefficient of $\sin\theta$ represents the solution of $U_1(r)$, and solution of constant is $U_2(r)$. By combining the solutions of both $U_1(r)\sin\theta$ and $U_2(r)$, we get the solution of first-order velocity distribution.

Here, the below equation represents the solution of $U_1(r)$

$$\begin{aligned} U_1(r) &= \left(\frac{1}{368640\kappa^2 I_0(k)} E_{s,0} u_r r \delta \zeta \left(-184320\kappa^2 I_0(kr) + 368640 I_2(kr) + \kappa \left(\kappa (184320 + r^8 \kappa^6 (-10 + \kappa^2) + 60r^6 \kappa^4 (-8 + \kappa^2) \right. \right. \right. \\ &\quad \left. \left. \left. + 1920r^4 \kappa^2 (-6 + \kappa^2) + 23040r^2 (-4 + \kappa^2) \right) + 184320r I_3(kr) \right) \right) \\ &\quad + \frac{\left(E_{s,0} u_r r \kappa^3 \delta \zeta \left(-4 + \frac{r^2 \mu_1^2}{2} - \frac{r^4 \mu_1^4}{24} + \frac{r^6 \mu_1^6}{768} - \frac{r^8 \mu_1^8}{46080} + 4J_0(r\mu_1) \right) (\kappa I_2(k) J_1(r\mu_1) + \mu_1 I_1(k) J_2(\mu_1)) \right)}{\left(4\mu_1 (\kappa^2 + \mu_1^2)^2 I_0(k) J_0(\mu_1) \right)} \\ &\quad + \frac{\left(E_{s,0} u_r r \kappa^3 \delta \zeta \left(-4 + \frac{r^2 \mu_2^2}{2} - \frac{r^4 \mu_2^4}{24} + \frac{r^6 \mu_2^6}{768} - \frac{r^8 \mu_2^8}{46080} + 4J_0(r\mu_2) \right) (\kappa I_2(k) J_1(\mu_2) + \mu_2 I_1(k) J_2(\mu_2)) \right)}{\left(4\mu_2 (\kappa^2 + \mu_2^2)^2 I_0(k) J_0(\mu_2) \right)} \\ &\quad + \frac{1}{16} r \delta \left(-3 + 3r^2 + 8E_{s,0} u_r \zeta - \frac{E_{s,0} u_r \phi \left(368640 I_2(k) + \kappa \left(92160\kappa + 11520\kappa^3 + 1440\kappa^5 + 50\kappa^7 + \kappa^9 + 184320 I_3(k) \right) \right)}{23040\kappa^2 I_0(k)} \right) \\ &\quad - \frac{\left(4E_{s,0} u_r \kappa^3 \zeta \left(-4 + \frac{\mu_1^2}{2} - \frac{\mu_1^4}{24} + \frac{\mu_1^6}{768} - \frac{\mu_1^8}{46080} + 4J_0(\mu_1) \right) (\kappa I_2(k) J_1(\mu_1) + \mu_1 I_1(k) J_2(\mu_1)) \right)}{\left(\mu_1 (\kappa^2 + \mu_1^2)^2 I_0(k) J_0(\mu_1) \right)} \\ &\quad - \frac{\left(4E_{s,0} u_r \kappa^3 \zeta \left(-4 + \frac{\mu_2^2}{2} - \frac{\mu_2^4}{24} + \frac{\mu_2^6}{768} - \frac{\mu_2^8}{46080} + 4J_0(\mu_2) \right) (\kappa I_2(k) J_1(\mu_2) + \mu_2 I_1(k) J_2(\mu_2)) \right)}{\left(\mu_2 (\kappa^2 + \mu_2^2)^2 I_0(k) J_0(\mu_2) \right)} \Big) \Big) \tag{49} \end{aligned}$$

Here, the below equation represents the solution of $U_2(r)$

$$\begin{aligned}
 U_2(r) = & \frac{1}{576\pi\kappa I_0(k)^2} S \left(576E_{s,0}\pi u_r \phi I_0(k)^2 - 576E_{s,0}\pi u_r \phi I_0(k)I_0(kr) - 288E_{s,0}\pi u_r \kappa \phi I_0(k)I_1(k) \right. \\
 & + 144E_{s,0}^2\pi u_r^2 \kappa^4 \phi^2 I_1(k)^2 + 288E_{s,0}\pi u_r r \kappa \phi I_0(k)I_1(kr) - 144E_{s,0}^2\pi u_r^2 r^2 \kappa^4 \phi^2 I_1(kr)^2 \\
 & - 144E_{s,0}^2\pi u_r^2 \kappa^4 \phi^2 I_0(k)I_2(k) + 144E_{s,0}^2\pi u_r^2 r^2 \kappa^4 \phi^2 I_0(kr)I_2(kr) \\
 & \left. - 9E_{s,0}^2\pi u_r^2 \kappa^6 \phi^2 \left(1 + \frac{2\kappa^2}{9} + \frac{5\kappa^4}{256} + \frac{7\kappa^6}{7200} \right) + 9E_{s,0}^2\pi u_r^2 r^4 \kappa^6 \phi^2 \left(1 + \frac{2\kappa^2 r^2}{9} + \frac{5\kappa^4 r^4}{256} + \frac{7\kappa^6 r^6}{7200} \right) \right). \tag{50}
 \end{aligned}$$

It needs to be pointed out that the streaming potential ($E_{s,0}$) appearing in the above velocity field is unknown. It can be determined by setting the electro-neutrality condition as followings.

3.3 Analysis of Streaming Potential

Another electrokinetic transport phenomenon is the streaming potential effect. Streaming current is the electric current generated by the movement of charged particles. Due to the pressure driven within the microtube, the charged particles drive a net charge accumulation inside the EDL, leading to current flow in the opposite direction. The flow of free electrons through the microtube is referred to as conduction current. The rate of flow is determined by the quantity of charge passing through a specific point in the circuit over a unit of time. When net charges in the EDL accumulate in a direction opposing the microtube flow, it results in a downstream potential greater than the upstream potential, ultimately giving rise to a potential difference known as streaming potential [12]. The presence of streaming potential leads to a reduction in the fluid flow velocity within the microtube, consequently causing an increase in viscosity. This phenomenon is termed the electro-viscosity effect. Here, we need to note that in a curved microtube, the streaming potential and pressure gradient are not uniform throughout the tube. Therefore, in addition the purely pressure-driven velocity is adopted, denoted by \tilde{u}_p , which can be seen in electrokinetic energy conversion.

Charged ions that have accumulated in the downstream region might cause a conduction current, denoted by the symbol \tilde{I}_c . Basically $\tilde{I}_{ionic} = \tilde{I}_s + \tilde{I}_c$. To remain the fluid system electrically neutral, the conduction current and the streaming must remain in a condition of dynamic equilibrium and also for pressure-driven transport, \tilde{I}_{ionic} becomes identically zero at steady state. Therefore, $\tilde{I}_s + \tilde{I}_c = 0$. This allows one to calculate the streaming potential, which is denoted by E_s . Poisson–Boltzmann distribution can be employed to calculate total ionic current.

$$\begin{aligned}
 \tilde{I}_{ionic} = & \tilde{I}_s + \tilde{I}_c \\
 = & e z_v \int_0^{2\pi} \left(\int_0^a (n_+ \tilde{U}_{\phi^+} - n_- \tilde{U}_{\phi^-}) r dr \right) d\theta = 0, \tag{51}
 \end{aligned}$$

$$\begin{aligned}
 \tilde{U}_{\phi^+} = & (\tilde{U}_{\phi^+}) + \frac{R}{R + r \sin\theta} \left(\frac{e z_v \tilde{E}_s}{f_+} \right), \tilde{U}_{\phi^-} \\
 = & (\tilde{U}_{\phi^-}) - \frac{R}{R + r \sin\theta} \left(\frac{e z_v \tilde{E}_s}{f_-} \right). \tag{52}
 \end{aligned}$$

where \tilde{U}_{ϕ^+} and \tilde{U}_{ϕ^-} represents the axial velocities of cations and anions. $\left(\frac{e z_v \tilde{E}_s}{f_{\pm}} \right)$ represents electromigrative velocity, and $f_+ = f_- = f$ is the ionic friction coefficient for cations and anions. \tilde{E}_s represents dimensionalised streaming potential.

By substituting the bulk electrolyte concentration, axial velocities, and non-dimensional variables in Eq. (51), it leads to dimensionless Ionic current. By using this calculation, we solve for streaming potential.

$$\begin{aligned}
 -2n_0 e z_v a^2 u_{p,0} \left(\int_0^{2\pi} \left(\int_0^1 (\psi_e u) r dr \right) d\theta \right. \\
 \left. + M u_r E_s \int_0^{2\pi} \left(\int_0^1 \frac{r}{1 + \delta r \sin\theta} dr \right) d\theta \right) = 0, \tag{53}
 \end{aligned}$$

$$\begin{aligned}
 -M u_r E_s \int_0^{2\pi} \left(\int_0^1 \frac{r}{1 + \delta r \sin\theta} dr \right) d\theta \\
 = \int_0^{2\pi} \left(\int_0^1 (\psi_e u) r dr \right) d\theta. \tag{54}
 \end{aligned}$$

$$\int_0^{2\pi} \left(\int_0^1 \frac{r}{1 + \delta r \sin\theta} dr \right) d\theta = \pi, \tag{55}$$

$$-M u_r E_s \pi = \int_0^{2\pi} \left(\int_0^1 (\psi_e u) r dr \right) d\theta. \tag{56}$$

where $M = \frac{e^2 (z_v)^2 \mu}{\epsilon \kappa_B T f}$ represents the ionic Peclet number, which is a dimensionless parameter. By again substituting the perturbation expansions, we derive zeroth-order poten-

tial of streaming potential. We omit to find the streaming potential of first order, since it was not in the velocity distribution equation. This means that the curvature of the tube has no first-order effect on the streaming potential at the centre line of the tube.

$$\varepsilon^0 : -\pi M u_r E_{s,0} = 2\pi \int_0^1 (\psi_0(r) u_0(r)) r dr, \tag{57}$$

$$-\pi M u_r E_{s,0} = 2\pi \int_0^1 \left(\varphi \frac{I_0(kr)}{I_0(k)} \left(\frac{1-r^2}{4} + \varphi u_r E_{s,0} \left(\frac{I_0(kr)}{I_0(k)} - 1 \right) \right) \right) r dr, \tag{58}$$

$$E_k = \frac{\left(\frac{\rho_e}{(\delta a)^2} \right) \frac{\mu}{f} (M E_{s,0} \mu u_{e,0})^2 (\pi (4 + \delta^2))}{\left(\frac{1}{8} + \frac{\varepsilon}{I_0(k)} \left(\left(\frac{1}{64} + \frac{\lambda}{32} + \frac{3k^2}{6400} + \frac{k^4}{100,352} + \frac{k^6}{7,962,624} \right) \sin\theta \right) + \left(\frac{S}{72} \right) \right)}. \tag{64}$$

$$-M u_r E_{s,0} = \varphi \frac{I_2(k)}{k^2 I_0(k)} + \varphi^2 u_r E_{s,0} \left(1 - \frac{2I_1(k)}{k I_0(k)} - \left(\frac{I_1(k)}{I_0(k)} \right)^2 \right), \tag{59}$$

$$E_{s,0} = \frac{-\varphi I_2(k)}{k^2 I_0(k) \left(M u_r + \varphi^2 u_r \left(1 - \frac{2I_1(k)}{k I_0(k)} - \left(\frac{I_1(k)}{I_0(k)} \right)^2 \right) \right)}. \tag{60}$$

Therefore, Eq. (60) represents the zeroth order of streaming potential. We use $E_{s,0}$ in the velocity equation to describe the flow in curved microtube.

3.4 Efficiency of Electrokinetic Energy Conversion

The streaming potential and electroosmosis involve the phenomena in the primary stage of the conversion of electrokinetic energy. As it was discussed in the previous section, streaming potential is the process by which an electrical potential difference is produced as a result of the movement of fluid through a microtube. On the other hand, electroosmosis refers to the movement of a fluid, that is induced by the application of an electric field. This flow can be utilised to generate electrical energy. The term “electrokinetic energy conversion” more commonly refers to converting the kinetic energy of fluid flow into electrical energy.

The efficiency of electrokinetic energy conversion E_k is defined as:

$$E_k = \frac{\widetilde{\text{Power}}_{\text{out}}}{\widetilde{\text{Power}}_{\text{in}}}, \tag{61}$$

where $\widetilde{\text{Power}}_{\text{out}} = \frac{e z v}{4} \int_0^{2\pi} \left(\int_0^a (n_+ - n_-) \frac{e z v}{f} \left(\frac{\tilde{E}_s}{R + r \sin\theta} \frac{\partial \tilde{p}}{\partial \phi} \right) r dr \right) d\theta,$ (62)

$$\widetilde{\text{Power}}_{\text{in}} = \int_0^{2\pi} \left(\int_0^a \left(\frac{-1}{R + r \sin\theta} \frac{\partial \tilde{p}}{\partial \phi} \right) \tilde{u}_p(r, \theta) r dr \right) d\theta. \tag{63}$$

The extra term $\left(\frac{1}{R+r \sin\theta} \right)$ is due to curvedness of the microtube. Here, we solve Eq. (60) by making dimensionless form

The derivation of EKEC is briefly discussed in “[Appendix C](#)”.

3.5 Estimation of Volumetric Flow Rate

To find the flow rate of this present study, we integrate the asymptotic solution for the velocities over cross section of the tube. The flow rate in a curved microtube could be greater than in a straight microtube with identical pressure gradient and cross-sectional shape. Here, we use the velocity equations of zeroth order and first order. Since the velocity equations are dimensionless, we obtain dimensionless volumetric flow rate as

$$Q = \int_0^{2\pi} \left(\int_0^1 u(r, \theta) r dr \right) d\theta, \tag{65}$$

$$Q = \int_0^{2\pi} \left(\int_0^1 (u_0(r)) r dr \right) d\theta + \varepsilon \int_0^{2\pi} \left(\int_0^1 (U_1(r) \sin\theta + U_2(r)) r dr \right) d\theta = Q_0 + \varepsilon Q_1. \tag{66}$$

To find the volumetric flow rate, we solved the above equation by using Mathematica. The streaming potential $E_{s,0}$ is used for the derivation. The first-order term of flowrate is neglected since the streaming potential $E_{s,1}$ was neglected in velocity distribution and also the integral of cross section with $\sin\theta$ is calculated to be zero. Therefore, the volumetric flowrate is calculated for the zeroth order.

$$\begin{aligned}
 Q = & \frac{\pi}{8} + (\pi S\phi^2(-138240(-4M\kappa + \kappa(4 + \kappa^2)\phi^2)I_0(k)^3 + 2\kappa^4(5760 + 1440\kappa^2 + 135\kappa^4 + 7\kappa^6 \\
 & + 11520\left(1 + \frac{3\kappa^2}{16} + \frac{\kappa^4}{64} + \frac{7\kappa^6}{9216}\right) - 5760\left(1 + \frac{\kappa^2}{4} + \frac{3\kappa^4}{128} + \frac{7\kappa^6}{5760}\right)\phi^2 I_1(k) + 138,240\kappa\left(\kappa^2\left(\frac{1}{2} + \frac{\kappa^2}{24} + \frac{\kappa^4}{768} + \frac{\kappa^6}{46,080}\right)\right. \\
 & \left. - 4\left(1 + \frac{\kappa^2}{8} + \frac{\kappa^4}{192} + \frac{\kappa^6}{9216}\right)\right)\phi^2 I_1(k)^2 - 552,960\kappa^2\phi^2 I_1(k)^3 + 138,240I_0(k)^2\left(\kappa\kappa^2\left(\frac{1}{2} + \frac{\kappa^2}{24} + \frac{\kappa^4}{768} + \frac{\kappa^6}{46,080}\right)\right. \\
 & \left. - 4\left(1 + \frac{\kappa^2}{8} + \frac{\kappa^4}{192} + \frac{\kappa^6}{9216}\right)\right)(M - \phi^2) + (-2M\kappa^2 + 2(4 + 3\kappa^2)\phi^2)I_1(k) - \phi^2 I_0(k)(5760\kappa^5 + 1440\kappa^7 + 135\kappa^9 \\
 & + 7\kappa^{11} + 11,520\kappa^5\left(1 + \frac{3\kappa^2}{16} + \frac{\kappa^4}{64} + \frac{7\kappa^6}{9216}\right) - 5760\kappa^5\left(1 + \frac{\kappa^2}{4} + \frac{3\kappa^4}{128} + \frac{7\kappa^6}{5760}\right) \\
 & - 276,480\kappa^2\left(\frac{1}{2} + \frac{\kappa^2}{24} + \frac{\kappa^4}{768} + \frac{\kappa^6}{46080}\right)I_1(k) + 1,105,920\left(1 + \frac{\kappa^2}{8} + \frac{\kappa^4}{192} + \frac{\kappa^6}{9216}\right)I_1(k) + 552,960\kappa I_1(k)^2 \\
 & - 138,240\kappa^3 I_1(k)^2)I_2(k))/ (552,960\kappa^2(\kappa(M - \phi^2)I_0(k)^2 + 2\phi^2 I_0(k)I_1(k) + \kappa\phi^2 I_1(k)^2)^2) \\
 & - \frac{\pi\phi^2 I_2(k)^2}{\kappa(\kappa(M - \phi^2)I_0(k)^2 + 2\phi^2 I_0(k)I_1(k) + \kappa\phi^2 I_1(k)^2)}. \tag{67}
 \end{aligned}$$

Here, we presume an EDL of infinite thickness, denoted by $k \rightarrow \infty$. Assuming an infinitely thin EDL and an $I_0(k) \approx I_1(k)$, we obtain an approximation of $\frac{\pi}{8}$ for the zeroth-order flow rate.

4 Results and Discussion

In the preceding section, we derived analytical solutions for various aspects including the potential distribution within the electrical double layer (EDL), velocity distribution, streaming potential, and efficiency of electrokinetic energy conversion, as well as the volumetric flow rate of an incompressible Bingham plastic fluid in a curved microtube. All these analytical solutions are derived up to first order by using perturbation technique. To ensure the accuracy and relevance of our results, we carefully selected key parameters. The microtube radius (R) ranged from 100 to 200 μm [44]. The thickness of the electric double layer (EDL), denoted by κ , varied from 0.25 to 1 μm . [44, 45] Additionally, the applied electrical fields in the flow (E_0) directions were set between 0 and 2×10^4 V/m [45, 46]. Lastly, the wall zeta potential ($\tilde{\zeta}$) for the curved microtube was determined to be between -18 and -12.5 mV. The parameter $u_r = 1$ is considered, and it indicates the strength of comparable pressure electroosmotic velocity to the pressure-driven velocity. In order to obtain meaningful results, it is necessary to establish the relevant ranges of these dimensionless parameters based on pertinent physical variables (Table 1).

4.1 Analysis on the Profiles of EDL Potential Distribution

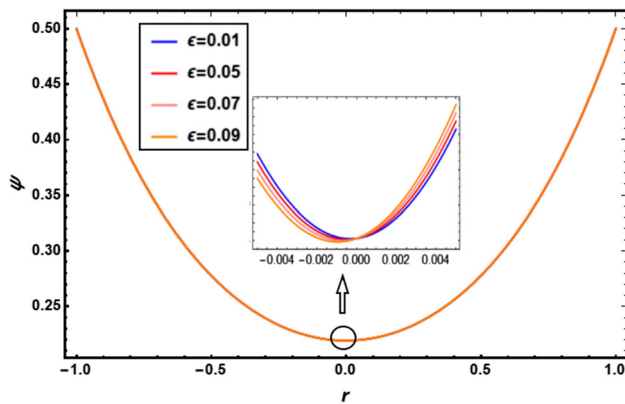
This section details the profiles of EDL potential distribution by comparing with different parameters values of EDL thickness, zeta potential, curvature ratio, perturbation parameter.

Here in Fig. 2, the electrical double-layer (EDL) distribution is a function of radial position in a curved microtube. So, the distributions can change by depending on the Debye length. The Debye length (κ) describes about the range of electrostatic interactions close to the charged surface (κ) and represents the characteristic length scale of the electrical double layer. The considered electroosmotic parameter values are less than, equal to, and greater than radius, and the respective parameter values are taken as $\phi = 0.5$, $\delta = 0.5$, $\theta = \frac{\pi}{4}$. Based on these values, EDL profile varies. In case of low Debye length value, a plug-like uniform profile is found. In case of high value of Debye length, a wave like profile is seen for the zeroth order of EDL potential profile. Therefore, Fig. 2 represents the overall EDL profile, where the profile decreases rapidly in the centre. In such cases, there is no chance for the fluid to flow forward. Thus, a backflow is to be found at the centre of the microtube. As the value of Debye length increases, the profile of EDL decreases more rapidly.

The analytical solutions are obtained through perturbation method till first order. So, our results are concluded using perturbation technique. Figure 3 is resulted by using perturbation

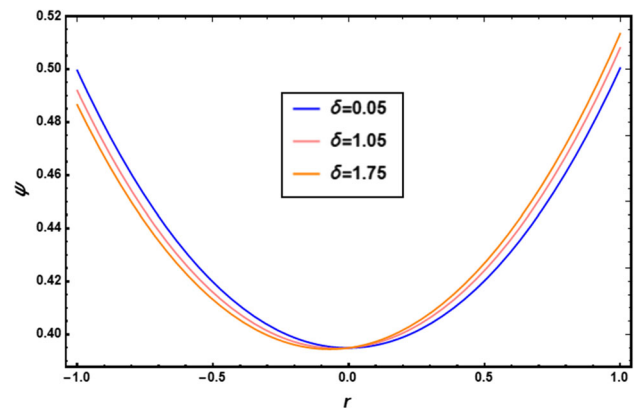
Table 1 Different parameters and its values [27, 47]

Parameter	Symbol	Value (Range in between)
Radius	r	1
EDL thickness	κ	0–20
Zeta potential	ζ	0–0.5
Curvature ratio	δ	0–2
Perturbation parameter	ε	0–0.1
Bingham parameter	S	0–1
Peclet number	M	0.01–10
Dimensionless-velocity scale (electroosmotic/pressure)	u_r	1

**Fig. 3** Variations of EDL distribution for different values of perturbation parameter

parameter $\varepsilon = 0.01, 0.05, 0.07, 0.09$, and the other parameter values are taken as $\phi = 0.5$, $\delta = 0.5$, $\theta = \frac{\pi}{4}$. Since the considered parameter values are very small, we can see the overlap for different values. But the truth behind is different. When we zoom the scale, one can see the profile more clearly. Initially, the EDL decreases with lower perturbation parameter value in the lower region of curvature but at the centre it changes its profile and start increasing in the upper region of curvature. Similarly, as the parameter value increases, EDL decreases and later from the centre the flow converges and starts increasing.

The curvature ratio is a dimensionless measurement used to express the bending nature of the system. The ratio of the radius of curvature of a microtube to the characteristic length of the tube is used to determine the curvature. To describe the geometric properties and behaviour of curved structures, the curvature ratio is useful since it gives information on the relative magnitude of curvature. Electroosmotic flow occurs when an external electric field is applied to the fluid. The flow in the curved microtube is influenced by its curvature, resulting in the generation of centrifugal force. The centrifugal force generates the secondary flow and impacts the boundary layers. In the channel core, the dominating inertial force

**Fig. 4** Variations of EDL distribution for different values of curvature ratio

causes a secondary flow from the inner to outer curve. However, near the walls, inertial force weakens due to viscosity and no-slip conditions. The radial pressure gradient causes a reverse secondary flow from outer to inner curve, aligning with mass conservation. Thus, centrifugal force impacts boundary layers as both source and reservoir. The interplay of opposing secondary flows forms two vortices in curved channels. In Fig. 4, the values of the curvature are in an increasing order where $\delta = 0.05, 1.05, 1.75$ and the other parameters are taken as $\phi = 0.5$, $\delta = 0.5$, $\theta = \frac{\pi}{4}$. Figure 4 depicts that as the curvature ratio is less, the EDL increases for radius less than 0 (lower wall region) and later it decreases for radius greater than zero (upper wall region). As the curvature increase, EDL decreases in near the lower wall and increase near the upper wall.

The measure of electric potential difference between the surface of a charged particle and the surrounding fluid is called the zeta potential (ζ -potential). It is a crucial metric for analysing the interaction of colloidal particles or surfaces in a fluid medium. In Fig. 4, the values of the curvature are in an increasing order where $\zeta = 0.1, 0.2, 0.3, 0.4$ and the other parameters are taken as $\phi = 0.5$, $\delta = 0.5$, $\theta = \frac{\pi}{4}$. Figure 5 demonstrates that the EDL profile is high for the higher values of zeta potential. As the zeta potential increases,

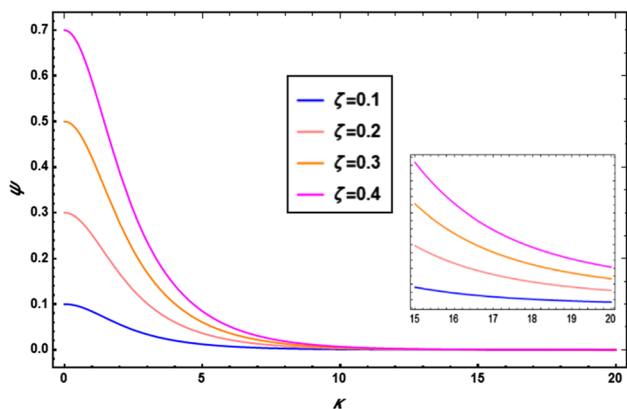


Fig. 5 Variations of EDL distribution for different values of zeta potential

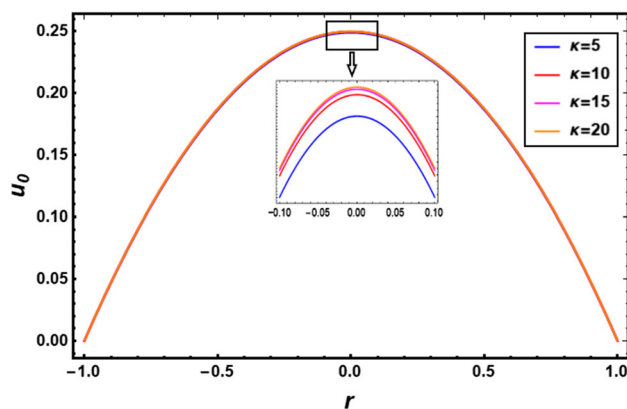


Fig. 7 Zeroth-order velocity profile for different values of Debye length at $M = 1$

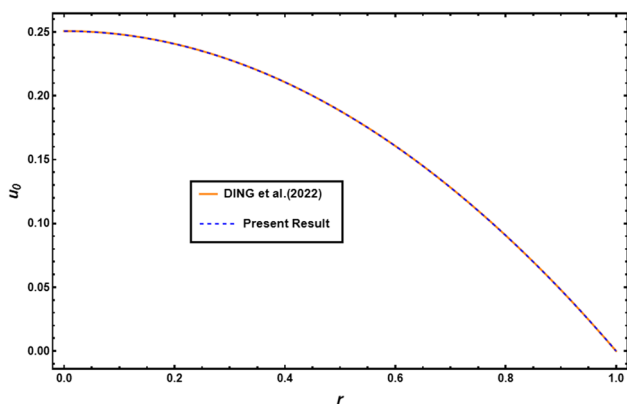


Fig. 6 Comparison of velocity profile with Ding et al. [9]

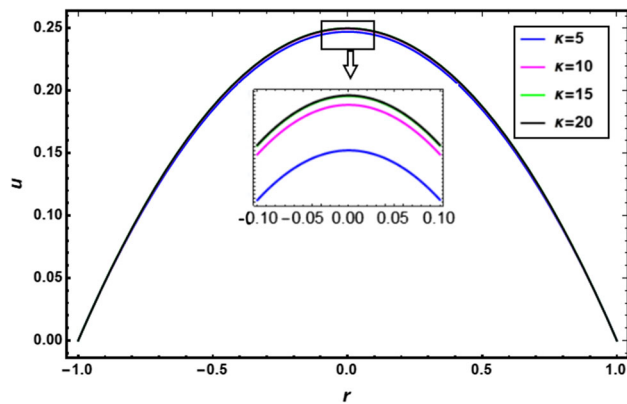


Fig. 8 Overall velocity profile for different values of Debye length at $M = 1$

the magnitude of the potential gradient across EDL increases and this leads to steeper electrical potential gradient within the EDL and also increase in zeta potential affects the distribution of charges and the structure of EDL leads to overall change in EDL potential. Later, there is a sudden drop in profile. As the zeta potential decreases, the width of EDL profile decreases more and more.

4.2 Analysis on the Profiles of Axial Velocity Distribution

This section details the profiles of velocity distribution by comparing with parameters and their values. The parameters include EDL thickness, zeta potential, curvature ratio and Peclet number. Validation of the present model is compared with the analytical work of Ding et al. [47]. Figure 6 compares the analytical results of zeroth-order velocity profile for the Newtonian fluid in a curved microtube and the flow of Bingham plastic fluid in a curved microtube for the values of $\phi = 0.9$, $\kappa = 10$, $u = 1$, $M = 10$. Validation presents that there is a better agreement between the present and previous

results. Thus, the validity of analytical model for the flow of Bingham plastic fluid in a curved tube is approved.

The velocity profile for zeroth order and overall axial velocity profile of the curved microtube are shown in Figs. 7 and 8. It displays that the velocity profile increases with the increase in electroosmotic parameter value. The reason behind this phenomenon is that the axial electric force in the inner area is larger than the outer region due to shorter arc length and this results to the increase in velocity. Due to electroosmosis, the velocity is affected by EDL in the broader section of the channel, resulting in the parabolic profiles. The EDL becomes more concentrated in a thinner layer near the wall, resulting in an amplified velocity gradient near the wall. Here, as κ value decreases, the flow becomes flattened. If the κ or M value increases, the streaming potential decreases and as a result there is no back flow in the velocity profile. The velocity profile is parabolic and its maximum point is 0.25 in the centre of cross section of the torus, whereas Fig. 9 illustrates the velocity profile for the first order. In the lower wall region, velocity is higher and positive. In upper wall region, the velocity profile decreases and negatively charged. We can

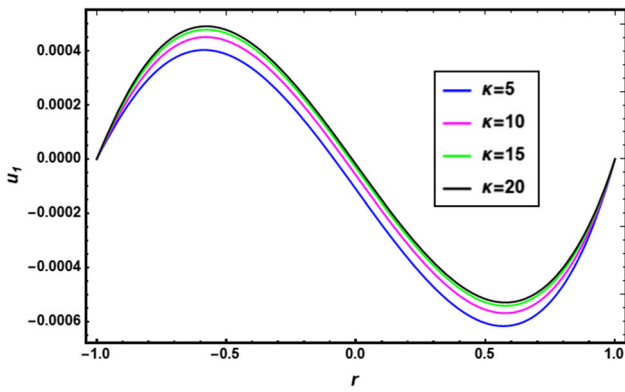


Fig. 9 First-order velocity profile for different values of Debye length at $M = 1$

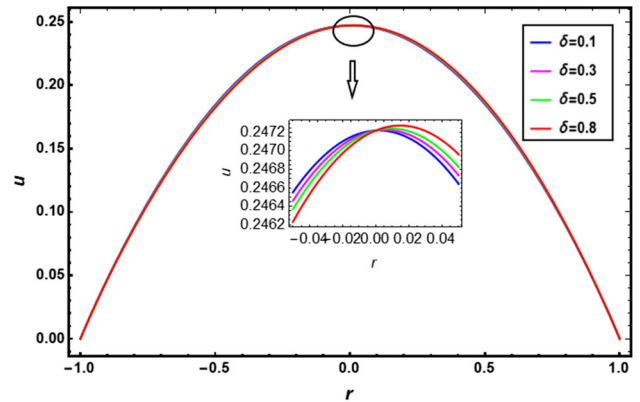


Fig. 11 Variation of velocity profile for different values of curvature ratio

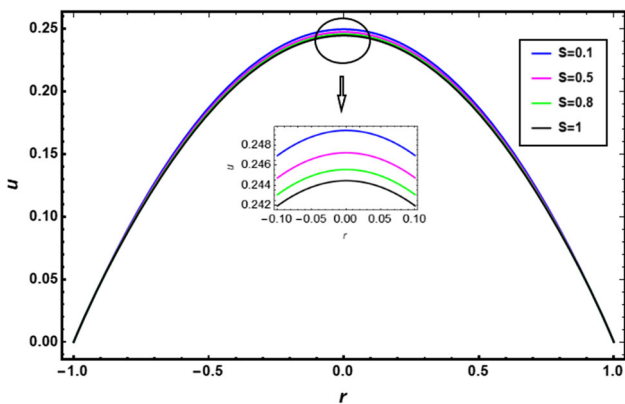


Fig. 10 Variation of velocity profile for different values of Bingham parameter at $M = 0.01$

alter the values of M as 0.01, 0.1, 10, so that there is a change in velocity profile for different values of κ .

Figure 10 depicts the velocity profile of fluid flow for different dimensionless values of Bingham parameter. By using Eqs. (42) and (46), we have plotted the graph for the fixed curvature $\delta = 1$. Figure 8 results that the fluid velocity decreases while the Bingham parameter increases. In the absence of yield stress, i.e. $S = 0$, the fluid behaves as a Newtonian fluid. As higher Bingham parameter indicates a higher resistance to flow, the remaining parameters are considered to be $\kappa = 5$, $u_r = 1$, $E_{s,0} = 0.2$, $\mu_1 0.56$, $\mu_2 0.578$, $\theta = \frac{\pi}{2}$, $M = 0.01$ that are kept as constant. Though we reduce the Bingham parameter to less than 0.1, the maximum velocity profile stops at 0.25 and cannot exceed more than that.

The velocity profile in Fig. 11 is affected by the change in curvature ratio by considering the Bingham parameter as constant at $S = 0.5$. As the curvature increases, the velocity reduces at the lower wall region. The velocity is also high at the plug flow, which is the centre region of the tube. But in the upper half of the tube, velocity increases with the increment of curvature value. If the curvature is zero, i.e. $\delta = 0$, the

velocity profile corresponds to a straight tube. The location of the point with the highest velocity is sufficiently distant from the upper half, since no-slip condition is the main consideration. However, it is not too near to the lower half, where the greater curvature would result in higher levels of stress.

In fluid dynamics, the Peclet number (M) is defined as the advection–diffusion ratio (ADR), and it is a dimensionless measure used to evaluate the balance between advection (convection) and diffusion. Since the considered fluid has plastic viscosity, the velocity distribution is influenced by Peclet number and characterises the ratio of advection to diffusion. Peclet number is directly proportional to the flow velocity. If the Peclet number is high, the velocity of the fluid flow increases. If the Peclet number is greater than one, then the motion of the fluid is determined mostly by its velocity rather than by diffusive factors, suggesting that advection dominates over diffusion. In such a scenario, the velocity field is more likely to have a uniform velocity distribution. However, in the opposite case, where the Peclet number is small ($M \ll 1$), diffusion becomes more important than advection. The yield stress and plastic viscosity of the fluid have a greater impact on the velocity distribution in this regime. As the Bingham plastic behaviour increases, a plug-like flow profile develops. The fluid has a constant velocity in a central area, but its motion is restricted towards the edges due to the yield stress. This causes the velocity gradient to increase towards the walls. We can clearly see in Fig. 12, for the values of $M = 1$ and $M = 10$ the velocity is equally distributed but as the ionic Peclet number increases, the flow velocity also increases.

4.3 Analysis on the Profiles of Volumetric Flow Rate

In the following section, we determine the volumetric flow rate with electroosmotic parameter κ for different Bingham parameter values of Peclet numbers.

Figures 13 and 14 illustrate dimensionless volumetric

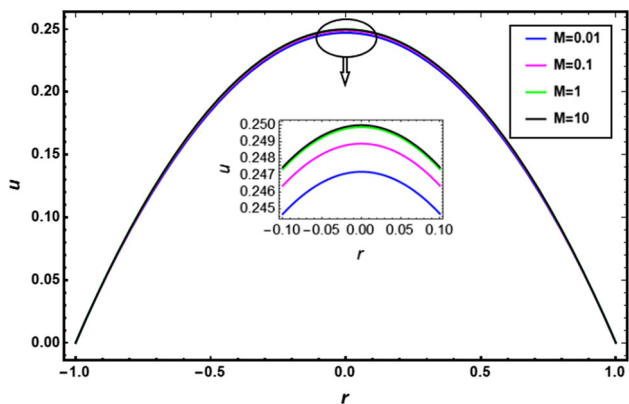


Fig. 12 Variation of velocity profile for different values of Peclet number

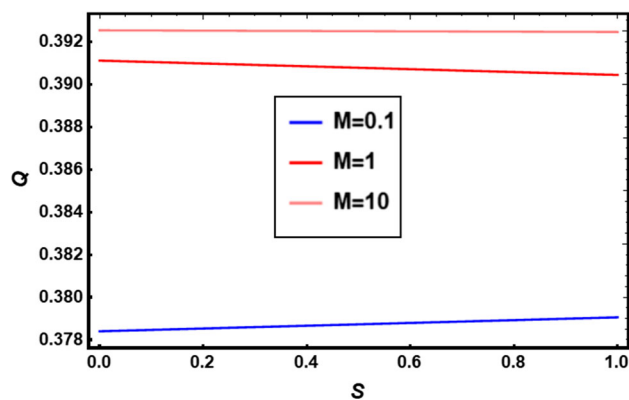


Fig. 15 Variation of volumetric flowrate with S for different values of M

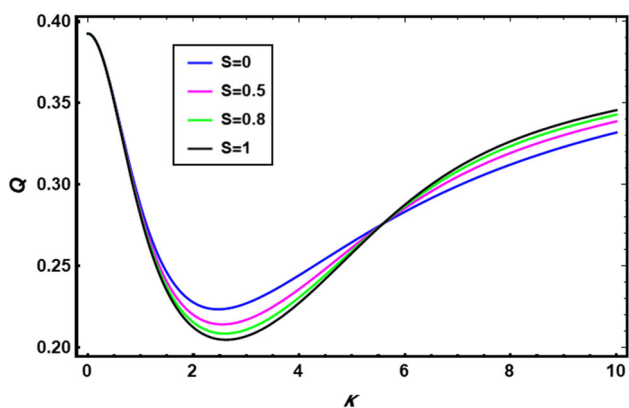


Fig. 13 Variation of volumetric flowrate for different values of Bingham parameter

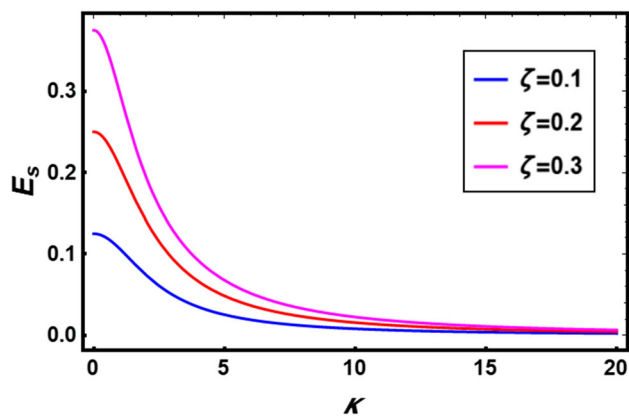


Fig. 16 Variation of streaming potential for different values of zeta potential

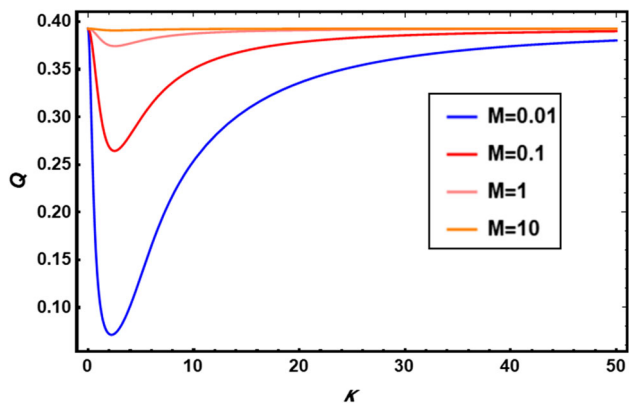


Fig. 14 Variation of volumetric flowrate for different values of Peclet number

flowrate. In Fig. 13, for the low values of electroosmotic parameter, the flow rate is decreased with the enhancing nature of Bingham parameter. Due to streaming potential, there is a sudden reduction in flow rate. As $\kappa > 5.5$, flow rate

is increased with respect to the increase of Bingham parameter. In a curved microtube, the flow rate of electrokinetic flow is always larger than straight tube though it has same cross section and pressure gradient. In curved microtube, the pressure gradient is along the centre of microtube. For the low values of ionic Peclet number, there is decrease in flow rate and later as there is a simultaneous increase in Debye length and Ionic Peclet number we can observe a uniform flow rate in Fig. 14.

The impact of Peclet number on flow rate is shown in Fig. 15. As the Peclet number increases, the flowrate decreases, and the flow profile of a fluid with a low Peclet number resembles a plug, with the fluid moving at a constant velocity in the central area and confined to a smaller volume near the boundaries due to yield stress.

4.4 Analysis on the Profiles of Streaming Potential

The streaming potential field and streaming current are generated by the external pressure gradient, which causes the fluid to flow. Figure 16 depicts the variation compared to

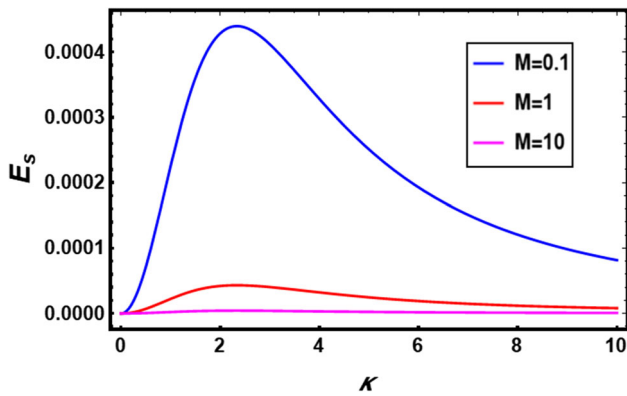


Fig. 17 Variation of streaming potential for different values of ionic Peclet number

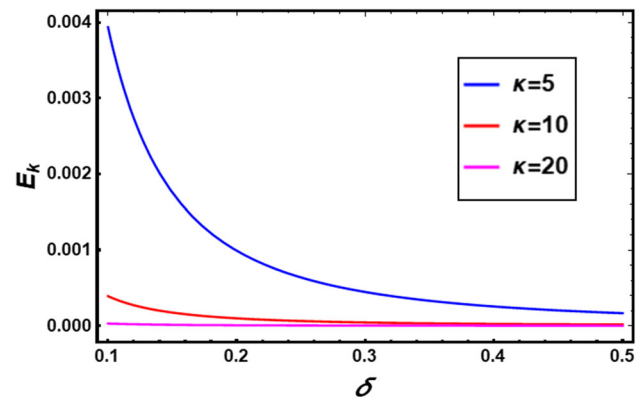


Fig. 18 Variation of electrokinetic energy conversion for different values of Debye length

the dimensionless streaming potential with the electroosmotic parameter κ (dimensionless) for different values of zeta potential. For small values of κ , the streaming potential field is very large, the variation of the dimensionless streaming potential increases initially with the increase in normalised zeta potential, later then there is a sudden decrease due to back flow. With the increase in κ , streaming potential decreases in magnitude and pressure-driven flow dominates the electroosmotic flow. Similarly for the values of larger Ionic Peclet number, it lowers the streaming potential in Fig. 17. Increase in the value of M (ionic Peclet number) reduces the fluid flow and it is not fully developed, and thus, the streaming potential decreases. This happens because the contribution of pressure to the flow is not much great as contribution of electroosmotic flow in the opposite direction, where the ions migrate in EDL and leads the fluid to backflow near the walls.

4.5 Analysis on the Profiles of Electrokinetic Energy Conversion

The variation of the electrokinetic energy conversion efficiency E_k with the curvature ratio for different values of the dimensionless κ is depicted in Fig. 18. It can be seen that the increase in values of dimensionless κ is easy to cause the smaller electrokinetic energy conversion efficiency. Due to enhancement in values of κ , it makes the energy conversion incomplete and decreases the efficiency of electrokinetic energy conversion. With the increase of κ , the change E_k becomes asymmetric, and it decreases.

The variation of the electrokinetic energy conversion efficiency E_k with curvature ratio δ for different values of Bingham parameters is shown in Fig. 19. From this figure, we can clearly observe that the larger value of Bingham parameter leads to a smaller electrokinetic energy conversion efficiency. Increase in the value of Bingham parameter increases the viscosity of the Bingham plastic fluid, which makes the fluid to move slow and reduces the streaming

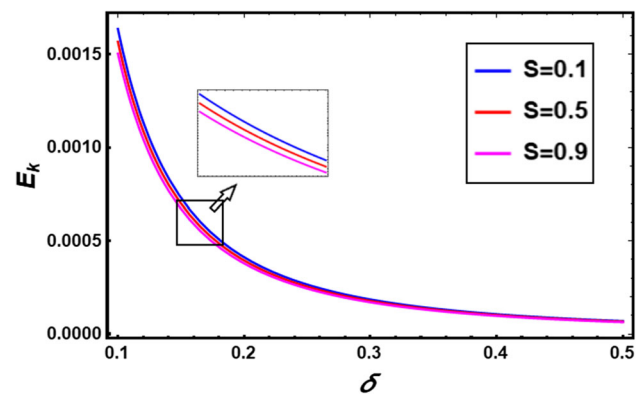


Fig. 19 Variation of electrokinetic energy conversion for different values of Bingham parameters

potential, and also there is a decrease in efficiency of electrokinetic energy conversion of the Bingham plastic fluid. Therefore, the E_k efficiency has a decreasing nature with the increase in the curvature ratio.

5 Conclusion

This paper comprehensively analyses EDL distribution, velocity distribution, fluid flow rate, streaming potential, and electrokinetic energy conversion efficiency driven by external pressure gradients and electric fields. These analyses are conducted under the assumption of a Bingham plastic fluid within a curved microtube featuring a circular cross section. By utilising the perturbation method, we derive the analytical solution for velocity and delve into the potential distribution across the electric double layer (EDL) as well as the velocity distribution concerning radius. These investigations encompass various values of parameters such as the Bingham parameter (S), electroosmotic parameter κ , zeta potential (ζ), curvature ratio (δ), and dimensionless Peclet number (M).

Analysis is done based on the variation of EDL with Debye length, perturbation parameter, curvature ratio, zeta potential. Also, analysis is done for variation of velocity distribution with Debye length, Bingham parameter, curvature ratio, and Peclet number. Volumetric flow rate analysis is conducted by different values of Bingham parameter and Peclet number. We analysed the streaming potential for different values of zeta potential and ionic Peclet number. Variation of electrokinetic energy conversion with different values of Debye length and Bingham parameter.

Significant findings emerge from our study, particularly in connection with applications associated with emerging technologies. Notably, alterations in volumetric flow rate, streaming potential, and electrokinetic energy conversion efficiency are observed under the influence of distinct parameters. A noteworthy trend emerges as the Bingham parameter value increases, leading to a reduction in velocity flow attributed to increased viscosity. As the curvature increases, the velocity reduces at the lower wall region. The velocity is also high at the plug flow, which is the centre region of the tube. Increase in the value of M (ionic Peclet number) reduces the fluid flow and it is not fully developed, and thus, the streaming potential decreases. Due to enhancement in values of Debye length, it makes the energy conversion incomplete and decreases the efficiency of electrokinetic energy conversion. The streaming potential, by opposing the flow, arises from the separation of charged particles inducing their own electric field. This electric field acts on the ions as if they were a liquid, enhancing friction and thus amplifying flow resistance. Additionally, an increase in the ionic Peclet number results in a narrower confinement within the flow.

These findings collectively underscore the intricate interplay between fluid dynamics, electric fields, and charge interactions in microscale environments, holding profound implications for various technological applications.

There are a number of real-world applications where the flow of Bingham plastic fluid in curved microtubes may be found across a variety of sectors. In the oil and gas industry, it is standard practice to transport Bingham plastic fluids, such as drilling muds and crude oil, along curved parts of pipelines. This is because of the high viscosity of these fluids. In Biomedical engineering, where the movement of these fluids in curved microchannels replicates physiological circumstances, making it useful for investigating blood flow in microvessels or constructing microfluidic devices for drug testing and administration. Another use of this technique is in the field of biomedical engineering. Operations in Mining and Mineral Processing, where Bingham plastic fluids are utilised in mining and mineral processing operations for the purpose of conveying slurries that include ores, tailings, and other particle materials. It is possible to increase the efficiency of mineral extraction operations by studying the flow

of these fluids in curved microtubes. This also helps minimise the amount of equipment wear and maintenance that is required.

Appendix A

Derivations of η_1 and h

H is referred as the intensity of deformation rate. It is difficult to calculate and the fact is that it takes simplest form when the motion is two-dimensional and symmetry. So here we consider simple assumptions to simplify h , then it makes effortless [27].

$$h = (2e_{ij}e_{ij})^{\frac{1}{2}} = 2^{\frac{1}{2}}(e_{rr}^2 + e_{\theta\theta}^2 + e_{\phi\phi}^2 + 2e_{r\theta}^2 + 2e_{r\phi}^2 + 2e_{\theta\phi}^2)^{\frac{1}{2}} \quad (68)$$

where e_{rr} , $e_{\theta\theta}$, $e_{\phi\phi}$, $e_{r\theta}$, $e_{r\phi}$, $e_{\theta\phi}$ are the rate of strain tensors.

The physical components [27] of rate of strain tensor are:

$$\begin{aligned} e_{rr} &= \frac{\partial U}{\partial r}; \quad e_{\phi\phi} = \frac{U \sin \theta + V \cos \theta}{R + r \cos \theta}; \quad e_{\theta\theta} = \frac{1}{r} \frac{\partial V}{\partial \theta} + \frac{U}{r} \\ e_{r\theta} &= \frac{1}{2} \left(\frac{1}{r} \frac{\partial V}{\partial r} + \frac{1}{r} \frac{\partial U}{\partial \theta} \right); \quad e_{r\phi} = \frac{1}{2} \left(\frac{\partial W}{\partial r} - \frac{W \sin \theta}{R + r \sin \theta} \right); \\ e_{\theta\phi} &= \frac{1}{2} \left(\frac{1}{r} \frac{\partial W}{\partial \theta} - \frac{W \cos \theta}{R + r \sin \theta} \right) \end{aligned} \quad (69)$$

Since $(U, V) = (0, 0)$ and $W(r, \theta)$ is independent of ϕ

$$h = 2^{\frac{1}{2}} \left(0 + 0 + 0 + 0 + 2e_{r\phi}^2 + 0 \right)^{\frac{1}{2}} \quad (70)$$

Therefore,

$$h \approx 2e_{r\phi} \quad (71)$$

$$\begin{aligned} h &\approx \left(\frac{\partial w}{\partial r} - \frac{w \sin \theta}{R + r \sin \theta} \right) = \left(\frac{\partial w}{\partial r} - \frac{\delta w \sin \theta}{a(1 + \delta r \sin \theta)} \right) \\ &= \left(\frac{\partial w}{\partial r} - \frac{\delta}{a} w \sin \theta (1 + \delta r \sin \theta)^{-1} \right) \\ &\approx \left(\frac{\partial w}{\partial r} - \frac{\delta}{a} w \sin \theta (1 - \delta r \sin \theta) \right) \end{aligned} \quad (72)$$

$(1 + \delta r \sin \theta)^{-1} \approx (1 - \delta r \sin \theta)$, Since δ is small we neglect higher-order terms.

Appendix B

Derivation of EDL and Axial Velocity

Conversion of dimension EDL to non-dimension EDL by using normalised variables:

$$\frac{\partial^2 \tilde{\psi}_e}{\partial r^2} + \frac{1}{r} \frac{\partial \tilde{\psi}_e}{\partial r} + \frac{\sin\theta}{(R+r\sin\theta)} \frac{\partial \tilde{\psi}_e}{\partial r} + \frac{1}{r^2} \frac{\partial^2 \tilde{\psi}_e}{\partial \theta^2} + \frac{\cos\theta}{r(R+r\sin\theta)} \frac{\partial \tilde{\psi}_e}{\partial \theta} = \frac{2n_0 z_v e}{\varepsilon} \left(\sinh \left(\frac{z_v e \tilde{\psi}_e}{k_B T} \right) \right) \quad (73)$$

$$\frac{\partial^2 \psi_e}{\partial r^2} + \frac{1}{r} \frac{\partial \psi_e}{\partial r} + \frac{\delta \sin\theta}{(1+\delta r \sin\theta)} \frac{\partial \psi_e}{\partial r} + \frac{1}{r^2} \frac{\partial^2 \psi_e}{\partial \theta^2} + \frac{\delta \cos\theta}{r(1+\delta r \sin\theta)} \frac{\partial \psi_e}{\partial \theta} = k^2 \psi_e \quad (74)$$

$(1 + \delta r \sin\theta)^{-1} \approx (1 - \delta r \sin\theta)$; Since δ is small, we neglect higher-order terms.

$$\frac{\partial^2 \psi_e}{\partial r^2} + \frac{1}{r} \frac{\partial \psi_e}{\partial r} + \delta \sin\theta (1 - \delta r \sin\theta) \frac{\partial \psi_e}{\partial r} + \frac{1}{r^2} \frac{\partial^2 \psi_e}{\partial \theta^2} + \frac{\delta \cos\theta}{r} (1 - \delta r \sin\theta) \frac{\partial \psi_e}{\partial \theta} = k^2 \psi_e \quad (75)$$

$$\frac{\partial^2 \psi_e}{\partial r^2} + \frac{1}{r} \frac{\partial \psi_e}{\partial r} + \delta \sin\theta \frac{\partial \psi_e}{\partial r} + \frac{1}{r^2} \frac{\partial^2 \psi_e}{\partial \theta^2} + \frac{\delta \cos\theta}{r} \frac{\partial \psi_e}{\partial \theta} = k^2 \psi_e \quad (76)$$

Conversion of dimension axial velocity to non-dimension axial velocity by using normalised variables:

$$\left(\eta_1 + \frac{\vartheta}{h} \right) \left[\left[\left(\frac{\partial}{\partial r} + \frac{1}{r} + \frac{2\sin\theta}{R+r\sin\theta} \right) \left(\frac{\partial w}{\partial r} - \frac{w \sin\theta}{R+r\sin\theta} \right) \right] + \left[\left(\frac{1}{r} \frac{\partial}{\partial \theta} + \frac{2\cos\theta}{R+r\sin\theta} \right) \left(\frac{1}{r} \frac{\partial w}{\partial \theta} - \frac{w \cos\theta}{R+r\sin\theta} \right) \right] \right] - \frac{1}{R+r\sin\theta} \frac{\partial P}{\partial \phi} - \frac{\tilde{\rho}_e}{R+r\sin\theta} \frac{\partial \tilde{\psi}_s}{\partial \phi} = 0 \quad (77)$$

$$\left(\eta_1 + \vartheta (h_{dl}^{-1}) \right) \frac{u_p}{a^2} \left[\left[\left(\frac{\partial}{\partial r} + \frac{1}{r} + \frac{2\delta \sin\theta}{1+\delta r \sin\theta} \right) \left(\frac{\partial u}{\partial r} - \frac{u \delta \sin\theta}{1+\delta r \sin\theta} \right) \right] + \left[\left(\frac{1}{r} \frac{\partial}{\partial \theta} + \frac{2\delta \cos\theta}{1+\delta r \sin\theta} \right) \left(\frac{1}{r} \frac{\partial u}{\partial \theta} - \frac{u \delta \cos\theta}{1+\delta r \sin\theta} \right) \right] \right] + \frac{u_p}{a^2} \left(\frac{\mu}{(1+\delta r \sin\theta)} \right) - \left(\frac{u_r E_s}{(1+\delta r \sin\theta)} \rho_e \right) = 0 \quad (78)$$

$$\eta_1 \left\{ \left[\left[\left(\frac{\partial}{\partial r} + \frac{1}{r} \right) \left(\frac{\partial u}{\partial r} - u \delta \sin\theta \right) + 2\delta \sin\theta \right] \left(\frac{\partial u}{\partial r} \right) \right] + \left[\left(\frac{1}{r} \frac{\partial}{\partial \theta} \left(\frac{1}{r} \frac{\partial u}{\partial r} - u \delta \sin\theta \right) + 2\delta \cos\theta \right) \left(\frac{\partial u}{\partial r} \right) \right] \right\} + \frac{u_p}{a^1} \vartheta \left(\frac{u_{p,0}}{a} \left(\frac{du}{dr} \right) \right) \left(\left[\left[\left(\frac{\partial}{\partial r} + \frac{1}{r} \right) \left(\frac{\partial u}{\partial r} - u \delta \sin\theta \right) + 2\delta \sin\theta \right] \left(\frac{\partial u}{\partial r} \right) \right] + \left[\left(\frac{1}{r} \frac{\partial}{\partial \theta} \left(\frac{1}{r} \frac{\partial u}{\partial r} - u \delta \sin\theta \right) + 2\delta \cos\theta \right) \left(\frac{\partial u}{\partial r} \right) \right] \right) + u \delta \sin\theta \left[\left[\left(\frac{\partial}{\partial r} + \frac{1}{r} \right) \left(\frac{\partial u}{\partial r} - u \delta \sin\theta \right) + 2\delta \sin\theta \right] \left(\frac{\partial u}{\partial r} \right) \right] + \left[\left(\frac{1}{r} \frac{\partial}{\partial \theta} \left(\frac{1}{r} \frac{\partial u}{\partial r} - u \delta \sin\theta \right) + 2\delta \cos\theta \right) \left(\frac{\partial u}{\partial r} \right) \right] \right] + (1 - \delta r \sin\theta) \left(\frac{\Delta P a^2}{R u_p} \right) - \frac{\varepsilon k_B T \rho_e}{z_v e} E_0 E_s \frac{(1 - \delta r \sin\theta)}{u_p} = 0 \quad (79)$$

$$\frac{u_p}{a^2} \eta_1 \left\{ \left[\left[\left(\frac{\partial}{\partial r} + \frac{1}{r} \right) \left(\frac{\partial u}{\partial r} - u \delta \sin\theta \right) + 2\delta \sin\theta \right] \left(\frac{\partial u}{\partial r} \right) \right] + \left[\left(\frac{1}{r} \frac{\partial}{\partial \theta} \left(\frac{1}{r} \frac{\partial u}{\partial r} - u \delta \sin\theta \right) + 2\delta \cos\theta \right) \left(\frac{\partial u}{\partial r} \right) \right] \right\} + \frac{u_p}{a^3} \vartheta \left(\frac{u_p}{a} \left(\frac{du}{dr} \right) \right) \left(\left[\left[\left(\frac{\partial}{\partial r} + \frac{1}{r} \right) \left(\frac{\partial u}{\partial r} - u \delta \sin\theta \right) + 2\delta \sin\theta \right] \left(\frac{\partial u}{\partial r} \right) \right] + \left[\left(\frac{1}{r} \frac{\partial}{\partial \theta} \left(\frac{1}{r} \frac{\partial u}{\partial r} - u \delta \sin\theta \right) + 2\delta \cos\theta \right) \left(\frac{\partial u}{\partial r} \right) \right] \right) + u \delta \sin\theta \left[\left[\left(\frac{\partial}{\partial r} + \frac{1}{r} \right) \left(\frac{\partial u}{\partial r} - u \delta \sin\theta \right) + 2\delta \sin\theta \right] \left(\frac{\partial u}{\partial r} \right) \right] + \left[\left(\frac{1}{r} \frac{\partial}{\partial \theta} \left(\frac{1}{r} \frac{\partial u}{\partial r} - u \delta \sin\theta \right) + 2\delta \cos\theta \right) \left(\frac{\partial u}{\partial r} \right) \right] \right] - \frac{(1 - \delta r \sin\theta) \partial P}{R \partial \phi} + \frac{\varepsilon k_B T \rho_e}{z_v e a^2} \left(\frac{1 - \delta r \sin\theta}{R} \right) (-R \tilde{E}_s) \left(\frac{E_0}{E_0} \right) = 0 \quad (80)$$

$$\left\{ \left[\left[\left(\frac{\partial}{\partial r} + \frac{1}{r} \right) \left(\frac{\partial u}{\partial r} - u \delta \sin\theta \right) + (2\delta \sin\theta) \right] \left(\frac{\partial u}{\partial r} \right) \right] + \left[\left(\frac{1}{r} \frac{\partial}{\partial \theta} \left(\frac{1}{r} \frac{\partial u}{\partial r} - u \delta \sin\theta \right) + 2\delta \cos\theta \right) \left(\frac{\partial u}{\partial r} \right) \right] \right\} + \frac{u_p}{a^1 \eta_1} \vartheta \left(\frac{u_{p,0}}{a} \left(\frac{du}{dr} \right) \right) \left(\left[\left[\left(\frac{\partial}{\partial r} + \frac{1}{r} \right) \left(\frac{\partial u}{\partial r} - u \delta \sin\theta \right) + 2\delta \sin\theta \right] \left(\frac{\partial u}{\partial r} \right) \right] + \left[\left(\frac{1}{r} \frac{\partial}{\partial \theta} \left(\frac{1}{r} \frac{\partial u}{\partial r} - u \delta \sin\theta \right) + 2\delta \cos\theta \right) \left(\frac{\partial u}{\partial r} \right) \right] \right) + u \delta \sin\theta \left[\left[\left(\frac{\partial}{\partial r} + \frac{1}{r} \right) \left(\frac{\partial u}{\partial r} - u \delta \sin\theta \right) + 2\delta \sin\theta \right] \left(\frac{\partial u}{\partial r} \right) \right] + \left[\left(\frac{1}{r} \frac{\partial}{\partial \theta} \left(\frac{1}{r} \frac{\partial u}{\partial r} - u \delta \sin\theta \right) + 2\delta \cos\theta \right) \left(\frac{\partial u}{\partial r} \right) \right] \right] + (1 - \delta r \sin\theta) \left(\frac{\Delta P a^2}{R u_p} \right) - \frac{\varepsilon k_B T \rho_e}{z_v e} E_0 E_s \frac{(1 - \delta r \sin\theta)}{u_p} = 0 \quad (81)$$

$$\begin{aligned}
 & -\delta r \sin\theta \left(\frac{\Delta P a^2}{R \eta_1 u_p} \right) \\
 & - \frac{\epsilon k_B T \rho_e}{z_v e \eta_1} E_0 E_s \frac{(1 - \delta r \sin\theta)}{u_p} = 0 \\
 & \left\{ \left[\left(\frac{\partial}{\partial r} + \frac{1}{r} \right) \left(\frac{\partial u}{\partial r} - u \delta \sin\theta \right) + (2\delta \sin\theta) \left(\frac{\partial u}{\partial r} \right) \right] \right. \\
 & + \left. \left\{ \left(\frac{1}{r} \frac{\partial}{\partial \theta} \left(\frac{1}{r} \frac{\partial u}{\partial r} - u \delta \sin\theta \right) + 2\delta \cos\theta \right) \left(\frac{\partial u}{\partial r} \right) \right\} \right\} \\
 & + \frac{u_p}{a^1 \eta_1} \vartheta \left(\frac{u_p}{a} \left(\frac{du}{dr} \right) \right) \left(\left[\left(\frac{\partial}{\partial r} + \frac{1}{r} \right) \left(\frac{\partial u}{\partial r} - u \delta \sin\theta \right) + 2\delta \sin\theta \right] \left(\frac{\partial u}{\partial r} \right) \right) \\
 & + \left\{ \left(\frac{1}{r} \frac{\partial}{\partial \theta} \left(\frac{1}{r} \frac{\partial u}{\partial r} - u \delta \sin\theta \right) + 2\delta \cos\theta \right) \left(\frac{\partial u}{\partial r} \right) \right\} \\
 & + u \delta \sin\theta \left[\left[\left(\frac{\partial}{\partial r} + \frac{1}{r} \right) \left(\frac{\partial u}{\partial r} - u \delta \sin\theta \right) + 2\delta \sin\theta \right] \left(\frac{\partial u}{\partial r} \right) \right] \\
 & + \left\{ \left(\frac{1}{r} \frac{\partial}{\partial \theta} \left(\frac{1}{r} \frac{\partial u}{\partial r} - u \delta \sin\theta \right) + 2\delta \cos\theta \right) \left(\frac{\partial u}{\partial r} \right) \right\} \\
 & + (1 \\
 & - \delta r \sin\theta) \left(\frac{u_p}{u_p} \right) \\
 & - \frac{u_e}{u_p} E_s (1 \\
 & - \delta r \sin\theta) \rho_e = 0
 \end{aligned}
 \tag{82}$$

$$\begin{aligned}
 & \frac{u_p}{a^2} \left(\eta_1 \right. \\
 & + \vartheta \left(\frac{u_p}{a} \left(\frac{du}{dr} + u \delta \sin\theta \right) \right) \left(\left[\left(\frac{\partial}{\partial r} + \frac{1}{r} + 2\delta \sin\theta \right) \left(\frac{\partial u}{\partial r} - u \delta \sin\theta \right) \right] \right) \\
 & + \left\{ \left(\frac{1}{r} \frac{\partial}{\partial \theta} + 2\delta \cos\theta \right) \left(\frac{1}{r} \frac{\partial u}{\partial r} - u \delta \cos\theta \right) \right\} \\
 & + \frac{u_p \mu}{a^2} (1 - \delta r \sin\theta) - (u_r E_s (1 - \delta r \sin\theta) \rho_e) = 0
 \end{aligned}
 \tag{83}$$

Appendix C

Derivation of EKEC

$$E_k = \frac{\widetilde{\text{Power}}_{\text{out}}}{\widetilde{\text{Power}}_{\text{in}}}
 \tag{84}$$

$$\begin{aligned}
 \widetilde{\text{Power}}_{\text{out}} &= \frac{e z_v}{4} \int_0^{2\pi} \left(\int_0^a (n_+ - n_-) \frac{e z_v}{f} \right. \\
 & \left. \left(\frac{\widetilde{E}_s}{R + r \sin\theta} \frac{\partial \widetilde{p}}{\partial \phi} \right) r dr \right) d\theta
 \end{aligned}
 \tag{85}$$

$$\widetilde{\text{Power}}_{\text{in}} = \int_0^{2\pi} \left(\int_0^a \left(\frac{-1}{R + r \sin\theta} \frac{\partial \widetilde{p}}{\partial \phi} \right) \widetilde{u}_p(r, \theta) r dr \right) d\theta
 \tag{86}$$

$$\begin{aligned}
 \widetilde{\text{Power}}_{\text{out}} &= \frac{1}{f} \left(\frac{\epsilon k_B T \rho_e}{z_v e a^2} \right) \frac{e z_v}{4} \int_0^{2\pi} \left(\int_0^1 \left(\frac{E_s E_0 R}{R(1 + \delta r' \sin\theta)} \frac{\partial \widetilde{p}}{\partial \phi} \right)^2 (ar') (adr') \right) d\theta
 \end{aligned}
 \tag{87}$$

$$\begin{aligned}
 \widetilde{\text{Power}}_{\text{out}} &= \frac{1}{f} \left(\frac{\epsilon k_B T \rho_e}{z_v e a^2} \right) \frac{e z_v}{4} \left(\frac{-z_v e \mu u_{e,0}}{\epsilon k_B T} \right)^2 (E_{s,0})^2 \left(\frac{1}{\delta} \right)^2 \\
 & \left(\frac{-a^2}{R} \frac{\partial \widetilde{p}}{\partial \phi} \right)^2 \int_0^{2\pi} \left(\int_0^1 (1 - \delta r' \sin\theta)^2 (r') (dr') \right) d\theta
 \end{aligned}
 \tag{88}$$

$$\begin{aligned}
 \widetilde{\text{Power}}_{\text{out}} &= \left(\frac{\rho_e}{(\delta a)^2} \right) \frac{1}{f} (M E_{s,0} \mu u_{e,0})^2 \\
 & \left(\frac{-a^2}{R} \frac{\partial \widetilde{p}}{\partial \phi} \right)^2 (\pi (4 + \delta^2))
 \end{aligned}
 \tag{89}$$

$$\begin{aligned}
 \widetilde{\text{Power}}_{\text{in}} &= \int_0^{2\pi} \left(\int_0^1 \left(\frac{-1}{R(1 + \delta r' \sin\theta)} \frac{\partial \widetilde{p}}{\partial \phi} \right) \left(\frac{-a^2}{\mu R} \frac{\partial \widetilde{p}}{\partial \phi} \right) u_p(r, \right. \\
 & \left. \theta) (ar') (adr') \right) d\theta
 \end{aligned}
 \tag{90}$$

$$\begin{aligned}
 \widetilde{\text{Power}}_{\text{in}} &= \frac{1}{\mu} \left(\frac{-a^2}{R} \frac{\partial \widetilde{p}}{\partial \phi} \right)^2 \int_0^{2\pi} \left(\int_0^1 u_p(r, \right. \\
 & \left. \theta) (1 - \delta r' \sin\theta) (r') (dr') \right) d\theta
 \end{aligned}
 \tag{91}$$

$$\begin{aligned}
 \widetilde{\text{Power}}_{\text{in}} &= \frac{1}{\mu} \left(\frac{-a^2}{R} \frac{\partial \widetilde{p}}{\partial \phi} \right)^2 \left(\frac{1}{8} \right. \\
 & + \frac{\epsilon}{I_0(k)} \left(\left(\frac{1}{64} + \frac{1}{32} + \frac{3k^2}{6400} + \frac{k^4}{100352} + \frac{k^6}{7962624} \right) \sin\theta \right) \\
 & \left. - \left(\frac{S}{72} \right) \right)
 \end{aligned}
 \tag{92}$$

$$E_k
 \tag{93}$$

$$\begin{aligned}
 &= \frac{\left(\frac{\rho_e}{(\delta a)^2} \right) \frac{\mu}{f} (M E_{s,0} \mu u_{e,0})^2 (\pi (4 + \delta^2))}{\left(-\frac{1}{8} + \frac{f}{I_0(k)} \left(\left(\frac{1}{64} + \frac{1}{32} + \frac{3k^2}{6400} + \frac{k^4}{100352} + \frac{k^6}{7962624} \right) \sin\theta \right) - \left(\frac{S}{72} \right) \right)}
 \end{aligned}$$

Acknowledgements This work was supported by SERB, Govt of India (Grant File No. MTR/2020/000585). The author (M. Reza) would like to acknowledge this support.

References

1. Cho, C.-C.; Chen, C.-L.; Chen, C.-K.: Mixing of non-Newtonian fluids in wavy serpentine microchannel using electrokinetically driven flow. *Electrophoresis* **33**, 743–750 (2012). <https://doi.org/10.1002/elps.201100496>
2. Berger, S.A.; Talbot, L.; Yao, L.S.: Flow in curved pipes. *Annu. Rev. Fluid Mech.* **15**, 461–512 (1983). <https://doi.org/10.1146/annurev.fl.15.010183.002333>
3. Stone, H.A.; Stroock, A.D.; Ajdari, A.: Engineering flows in small devices: microfluidics toward a lab-on-a-chip. *Annu. Rev. Fluid Mech.* **36**, 381–411 (2004). <https://doi.org/10.1146/annurev.fluid.36.050802.122124>

4. Dean, W.R.; Hurst, J.M.: Note on the motion of fluid in a curved pipe. *Mathematika* **6**, 77–85 (1959). <https://doi.org/10.1112/S0025579300001947>
5. Dean, W.R.: Fluid motion in a curved channel. *Proc. R. Soc. London. Ser. A Contain. Pap. Math. Phys. Charact.* **121**, 402–420 (1928). <https://doi.org/10.1098/rspa.1928.0205>
6. Messaris, G.A.T.; Karahalios, G.T.: Unsteady fluid flow in a slightly curved annular pipe: the impact of the annulus on the flow physics. *Phys. Fluids* (2017). <https://doi.org/10.1063/1.4976852>
7. Yang, W.H.; Zhang, J.Z.; Cheng, H.E.: The study of flow characteristics of curved microchannel. *Appl. Therm. Eng.* **25**, 1894–1907 (2005). <https://doi.org/10.1016/j.applthermaleng.2004.12.001>
8. Wang, C.Y.; Liu, Y.H.; Chang, C.C.: Analytical solution of electroosmotic flow in a semicircular microchannel. *Phys. Fluids* **20**, 063105 (2008). <https://doi.org/10.1063/1.2939399>
9. Ding, Z.; Jian, Y.; Tan, W.: Electrokinetic energy conversion of two-layer fluids through nanofluidic channels. *J. Fluid Mech.* **863**, 1062–1090 (2019). <https://doi.org/10.1017/jfm.2019.6>
10. Ding, Z.; Jian, Y.: Electrokinetic oscillatory flow and energy conversion of viscoelastic fluids in microchannels: a linear analysis. *J. Fluid Mech.* **919**, A20 (2021). <https://doi.org/10.1017/jfm.2021.380>
11. Luo, W.J.: Transient electroosmotic flow induced by DC or AC electric fields in a curved microtube. *J. Colloid Interface Sci.* **278**, 497–507 (2004). <https://doi.org/10.1016/j.jcis.2004.06.017>
12. Norouzi, M.; Biglari, N.: An analytical solution for Dean flow in curved ducts with rectangular cross section. *Phys. Fluids* (2013). <https://doi.org/10.1063/1.4803556>
13. Nekoubin, N.: Electroosmotic flow of power-law fluids in curved rectangular microchannel with high zeta potentials. *J. Nonnewton. Fluid Mech.* **260**, 54–68 (2018). <https://doi.org/10.1016/j.jnnfm.2018.06.005>
14. Sun, Y.J.; Jian, Y.J.; Chang, L.; Liu, Q.S.: Thermally fully developed electroosmotic flow of power-law fluids in a circular microchannel. *J. Mech.* **29**, 609–616 (2013). <https://doi.org/10.1017/jmech.2013.43>
15. Cheng, Z.; Ning, Z.; Dai, S.: The electroviscous flow of non-Newtonian fluids in microtubes and implications for nonlinear flow in porous media. *J. Hydrol.* (2020). <https://doi.org/10.1016/j.jhydrol.2020.125224>
16. Song, F.; Ding, H.; Huang, L.; Wang, Y.; Sun, Y.: Research on non-Newtonian characteristics of crude oil flow at micro-nano scale. *Phys. Fluids* (2023). <https://doi.org/10.1063/5.0145727>
17. Guo, Y.: Fluid-induced nonlinear vibration of a cantilevered microtube with symmetric motion constraints. *Shock. Vib.* (2020). <https://doi.org/10.1155/2020/8852357>
18. Sarabandi, A.H.; Moghadam, A.J.: Thermal analysis of power-law fluid flow in a circular microchannel. *J. Heat Transf.* (2017). <https://doi.org/10.1115/1.4035040>
19. Si, X.; Lei, X.; Xu, B.; Li, B.; Zhu, J.; Cao, L.: The periodic secondary flow of Oldroyd-B fluids driven by direct electric field in a rectangular curved channel. *Phys. Fluids* (2023). <https://doi.org/10.1063/5.0138394>
20. Moghadam, A.J.: Thermally developing flow induced by electroosmosis in a circular micro-channel. *Arab. J. Sci. Eng.* **39**, 1261–1270 (2014). <https://doi.org/10.1007/s13369-013-0717-8>
21. Riaz, A.; Saleem, K.; Raza, M.: Cilia-driven flow in a symmetric elliptical duct with electric double layer and thermal effects: exact solutions. *Arab. J. Sci. Eng.* **48**, 8189–8206 (2023). <https://doi.org/10.1007/s13369-023-07844-3>
22. Kumawat, C.; Sharma, B.K.; Al-Mdallal, Q.M.; Rahimi-Gorji, M.: Entropy generation for MHD two phase blood flow through a curved permeable artery having variable viscosity with heat and mass transfer. *Int. Commun. Heat Mass Transf.* (2022). <https://doi.org/10.1016/j.icheatmasstransfer.2022.105954>
23. Sun, Z.; Wu, T.; Yao, K.; Kasu, C.M.; Zhao, X.; Li, Z.; Gong, J.: Consolidation of soft clay by cyclic and progressive electroosmosis using electrokinetic geosynthetics. *Arab. J. Geosci.* (2022). <https://doi.org/10.1007/s12517-022-10380-3>
24. Shwedov, F.: La rigidité de liquides. *Rapp. Congr. Intern. Phys.* **1**, 478–486 (1900)
25. Bingham, E.C.: *Fluidity and Plasticity*, p. 147–439. McCraw-Hill Book Company, Inc., New York (1922)
26. Howard, A.B.: The yield stress—a review or ‘ $\pi\alpha\nu\tau\alpha$ ρ ι ’—everything flows? *J. Nonnewton. Fluid Mech.* **81**(1–2), 133–178 (1999)
27. Clegg, D.B.; Power, G.: Flow of a Bingham fluid in a slightly curved tube. *Appl. Sci. Res. Sect. A* **12**, 199–212 (1963). <https://doi.org/10.1007/BF03184640>
28. Roberts, T.G.; Cox, S.J.: An analytic velocity profile for pressure-driven flow of a Bingham fluid in a curved channel. *J. Nonnewton. Fluid Mech.* (2020). <https://doi.org/10.1016/j.jnnfm.2020.104278>
29. Shojaeian, M.; Karimzadehkhoei, M.; Koşar, A.: Experimental investigation on convective heat transfer of non-Newtonian flows of Xanthan gum solutions in microtubes. *Exp. Therm. Fluid Sci.* **85**, 305–312 (2017). <https://doi.org/10.1016/j.expthermflusci.2017.02.025>
30. Karabi, M.; Moghadam, A.J.: Non-Newtonian fluid flow and heat transfer in a semicircular microtube induced by electroosmosis and pressure gradient. *J. Heat Transf.* (2018). <https://doi.org/10.1115/1.4041189>
31. Tada, S.; Fukui, Y.; Oshima, S.; Yamane, R.: Effects of Bingham viscosity on flow in curved pipes. *JSME Int. J. Ser. B Fluids Therm. Eng.* **37**, 322–327 (1994). <https://doi.org/10.1299/jsmeb.37.322>
32. Moghadam, A.J.; Akbarzadeh, P.: Non-Newtonian fluid flow induced by pressure gradient and time-periodic electroosmosis in a microtube. *J. Braz. Soc. Mech. Sci. Eng.* **39**, 5015–5025 (2017). <https://doi.org/10.1007/s40430-017-0876-8>
33. Beltrame, P.: Drop train flow in a microtube. *Eur. Phys. J. Spec. Top.* **232**, 435–442 (2023). <https://doi.org/10.1140/epjs/s11734-023-00786-9>
34. Kumar, P.; Nagaraja, B.; Almeida, F.; AjayKumar, A.R.; Al-Mdallal, Q.; Jarad, F.: Magnetic dipole effects on unsteady flow of Casson–Williamson nanofluid propelled by stretching slippery curved melting sheet with buoyancy force. *Sci. Rep.* (2023). <https://doi.org/10.1038/s41598-023-39354-5>
35. Ng, C.O.; Qi, C.: Electroosmotic flow of a viscoplastic material through a slit channel with walls of arbitrary zeta potential. *Phys. Fluids* (2013). <https://doi.org/10.1063/1.4825368>
36. Bhandari, D.S.; Tripathi, D.; Narla, V.K.: Transient membrane kinematic model for viscoplastic fluids: periodic contraction in the microchannel. *Eur. Phys. J. Spec. Top.* (2022). <https://doi.org/10.1140/epjs/s11734-022-00655-x>
37. Zhang, X.; Shi, Y.; Kuang, S.; Zhu, W.; Cai, Q.; Wang, Y.; Wu, X.; Jin, T.: Microscale effects of Bingham-plastic liquid behavior considering electroviscous effects in nano- or micro-sized circular tubes. *Phys. Fluids* (2019). <https://doi.org/10.1063/1.5068774>
38. Shahsavari, S.; McKinley, G.H.: Mobility and pore-scale fluid dynamics of rate-dependent yield-stress fluids flowing through fibrous porous media. *J. Nonnewton. Fluid Mech.* **235**, 76–82 (2016). <https://doi.org/10.1016/j.jnnfm.2016.07.006>
39. Panwar, K.: Slip and no slip conditions in serpentine channel for Bingham fluid-numerical CFD investigation. *J. Graph. Era Univ.* (2023). <https://doi.org/10.13052/jgeu0975-1416.1114>
40. Al-Mdallal, Q.; Prasad, V.R.; Basha, H.T.; Sarris, I.; Akkurt, N.: Keller box simulation of magnetic pseudoplastic nano-polymer coating flow over a circular cylinder with entropy optimisation. *Comput. Math. Appl.* **118**, 132–158 (2022). <https://doi.org/10.1016/j.camwa.2022.05.013>
41. Yang, X.; Liang, Y.; Chen, W.: A fractal roughness model for the transport of fractional non-Newtonian fluid in microtubes. *Chaos*

- Solitons Fractals **126**, 236–241 (2019). <https://doi.org/10.1016/j.chaos.2019.06.015>
42. Yang, X.; Zhao, M.; Wang, S.; Xiao, Y.: Electro-osmotic flow of Maxwell fluid induced by an alternating electric field in curved rectangular microchannels. *Phys. Fluids* (2023). <https://doi.org/10.1063/5.0149681>
 43. Kontaxi, G.; Stergiou, Y.G.; Mouza, A.A.: Experimental study of bubble formation from a micro-tube in non-Newtonian fluid. *Micromachines* **12**, 1–10 (2021). <https://doi.org/10.3390/mi12010071>
 44. Reza, M.; Chamkha, A.J.; Rana, A.; Shit, G.C.: Anisotropic property of turbulent flow control through multiple stenosed microtubes. *Waves Random Complex Media* (2023). <https://doi.org/10.1080/17455030.2022.2164632>
 45. Oldroyd, J.G.: A rational formulation of the equations of plastic flow for a Bingham solid. *Math. Proc. Camb. Philos. Soc.* **43**, 100–105 (1947). <https://doi.org/10.1017/S0305004100023239>
 46. Oldroyd, J.G.: Two-dimensional plastic flow of a Bingham solid: a plastic boundary-layer theory for slow motion. *Math. Proc. Camb. Philos. Soc.* **43**, 383–395 (1947). <https://doi.org/10.1017/S0305004100023616>
 47. Ding, Z.; Tian, K.; Jian, Y.: Electrokinetic flow and energy conversion in a curved microtube. *Appl. Math. Mech.* **43**, 1289–1306 (2022). <https://doi.org/10.1007/s10483-022-2886-5>

Springer Nature or its licensor (e.g. a society or other partner) holds exclusive rights to this article under a publishing agreement with the author(s) or other rightsholder(s); author self-archiving of the accepted manuscript version of this article is solely governed by the terms of such publishing agreement and applicable law.